Significant Proximity and Cocatalyst Effects in Binuclear Catalysis for Olefin Polymerization

Hongbo Li, Charlotte L. Stern, and Tobin J. Marks*

Department of Chemistry, Northwestern University, Evanston, Illinois 60208-3113

Received May 7, 2005; Revised Manuscript Received August 8, 2005

ABSTRACT: We describe here the implementation of methylene-bridged binuclear "constrained geometry catalyst" (μ-CH_2-3,3′){(η^5-indenyl)[1-Me_2Si(^{t}BuN)]($ZrMe_2$)}$_2$ (C1-Zr_2) to produce high-M_w branched polyethylene. In ethylene homopolymerization, ∼70× increases in molecular weight are achieved with (C1-Zr_2) vs (μ-CH_2CH_2-3,3′){(η^5-indenyl)[1-Me_2Si(^{t}BuN)]($ZrMe_2$)}$_2$ (C2-Zr_2) under identical polymerization conditions using $(Ph_3C^+)_2$[1,4-$(C_6F_5)_3BC_6F_4B(C_6F_5)_3]^{2-}$ (B_2) as the cocatalyst for both. With MAO as the cocatalyst, ∼600× increases in polyethylene molecular weight are achieved with (μ-CH_2CH_2-3,3′){(η^5-indenyl)[1-Me_2Si(^{t}BuN)]($ZrCl_2$)}$_2$ (C2-Zr_2Cl_4) and (μ-CH_2-3,3′){(η^5-indenyl)[1-Me_2Si(^{t}BuN)]($ZrCl_2$)}$_2$ (C1-Zr_2Cl_4) vs mononuclear [1-Me_2Si(3-ethylindenyl)(^{t}BuN)]$ZrCl_2$ (Zr_1Cl_2). In the ethylene + 1-hexene copolymerization, C1-Zr_2 enchains 3× more 1-hexene than does C2-Zr_2 under identical polymerization conditions (B_2 as cocatalyst). With MAO as the cocatalyst, C2-Zr_2Cl_4 enchains 3.5× more, and C1-Zr_2Cl_4 4.2× more, 1-hexene than does Zr_1Cl_2. When the polar solvent C_6H_5Cl is used as the polymerization medium, dramatic compression in the dispersion of polymerization activities and molecular weights is found. Both homopolymerization and copolymerization results argue that achievable Zr−Zr spatial proximity significantly influences chain transfer rates and selectivity for comonomer enchainment and that such proximity effects are highly cocatalyst and solvent sensitive.

Intense recent research efforts have focused on discovering unique/more efficient catalytic processes benefiting from cooperative effects between active centers in multinuclear complexes, to ultimately mimic advantageous enzyme characteristics.[1] Regarding such effects in single-site polymerization catalysis,[2−4] we recently reported that the constrained geometry binuclear catalyst + binuclear cocatalyst combination C2-Zr_2 + B_2 (Chart 1) affords, via the modification of chain transfer pathway kinetics, significantly enhanced branching in ethylene homopolymerization and enhanced comonomer incorporation in ethylene + 1-hexene copolymerization vs mononuclear Zr_1 + B_1.[3f] Nevertheless, CGCZr catalysts typically produce unacceptably low-M_w polyolefins, raising the intriguing question of what effects closer metal−metal proximity and alternative cocatalysts might offer. More recently, we reported preliminary results showing that metal−metal proximity and cocatalyst structure have significant impact in terms of product molecular weight and comonomer enchainment selectivity.[3a] Here we discuss in full detail the range of catalyst structure, catalyst/cocatalyst ion pairing, and polymerization solvent effects operative in the polymerization processes. Specifically, single methylene-bridged (μ-CH_2-3,3′){(η^5-indenyl)[1-Me_2Si(^{t}BuN)]($ZrMe_2$)}$_2$ (C1-Zr_2) was synthesized to examine achievable metal−metal proximity effects, while sterically encumbered naphthyl-derivatized {1-Me_2Si[3-(1)-naphthylindenyl]-(^{t}BuN)}$ZrMe_2$ (N-Zr_1) was prepared to additionally probe catalytic center steric effects. It will be seen that poising the two metals into closer proximity can significantly enhance polyethylene molecular weight in ethylene homopolymerizations and α-olefin enchainment in ethylene + 1-hexene copolymerizations. Additionally, we find that when MAO is used as the cocatalyst, the bimetallic catalysts C1-Zr_2 and C2-Zr_2 afford even greater product M_w enhancement vs the mononuclear analogue.

* Corresponding author: e-mail t-marks@northwestern.edu.

Experimental Section

Materials and Methods. All manipulations of air-sensitive materials were performed with rigorous exclusion of O_2 and moisture in flamed Schlenk-type glassware on a dual-manifold Schlenk line or interfaced to a high-vacuum line (10^{-5} Torr) or in a nitrogen-filled Vacuum Atmospheres glovebox with a high capacity recirculator (<1 ppm of O_2). Argon and ethylene (Matheson, polymerization grade) were purified by passage through a supported MnO oxygen-removal column and an activated Davison 4A molecular sieve column. Ether solvents were purified by distillation from Na/K alloy/benzophenone ketyl. Hydrocarbon solvents were distilled under nitrogen from Na/K alloy. All solvents for high-vacuum line manipulations were stored in vacuo over Na/K alloy in Teflon-valve sealed bulbs. Deuterated solvents were obtained from Cambridge Isotope Laboratories (all ≥99 atom % D), freeze−pump−thaw degassed, over Na/K alloy, and stored in resealable flasks. Other nonhalogenated solvents were dried over Na/K alloy, and halogenated solvents were distilled from P_2O_5 and stored over activated Davison 4A molecular sieves. The reagents indene, Me_2SiCl_2, Bu^tNH_2, and ^{n}BuLi (1.6 M in hexanes) were purchased from Aldrich and used as received**.** The metal amide reagent $Zr(NMe_2)_4$ was purchased from Strem Chemicals and used as received. The comonomer 1-hexene (Aldrich) was dried over P_2O_5 and vacuum-transferred into a storage tube. Methylalumoxane (MAO, obtained as a toluene solution from Aldrich) was dried under high vacuum for 48 h to remove excess volatile aluminum alkyls before use.

Physical and Analytical Measurements. NMR spectra were recorded on either Varian VXR 500 (FT 500 MHz, ^{1}H; 125 MHz, ^{13}C) or VXR 400 (FT 400 MHz, ^{1}H; 100 MHz, ^{13}C) instruments. Chemical shifts for ^{1}H and ^{13}C spectra were referenced using internal solvent resonances and are reported relative to tetramethylsilane. ^{19}F NMR spectra were referenced to external $CFCl_3$. NMR experiments on air-sensitive samples were conducted in Teflon valve-sealed sample tubes (J. Young). Elemental analyses were performed by Oneida Research Services, Inc. Whitesboro, NY, or by Midwest Microlab, Indianapolis, IN. ^{13}C NMR assays of polymer microstructure

10.1021/ma050959c CCC: $30.25
Published on Web 09/30/2005

Chart 1

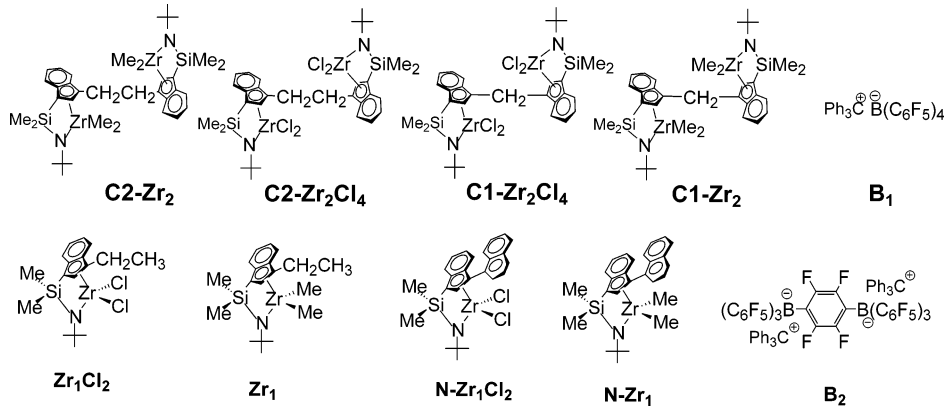

were conducted in a mixture (1:1 volume:volume) of 1,2,4-trichlorobenzene (containing 0.1 M $Cr(acac)_3$ solution) and 1,1,2,2-tetrachloroethane-d_2 at 120 °C. Signals were assigned according to the literature for polyethylene and ethylene + α-olefin copolymers.[5]

Gel permeation chromatographic (GPC) analysis was carried out on a Waters Alliance GPCV 2000 high-temperature instrument equipped with three Polymer Laboratories 10 μm mixed B columns operating at 145 °C and a refractive index detector. A flow rate of 1.0 mL/min was used, and HPLC grade 1,2,4-trichlorobenzene was employed as the eluent. Typically, 10 ± 1.0 mg of the sample was dissolved in 7.0 mL of TCB. The hot solutions were filtered using a 0.5 μm stainless steel filter. A polystyrene universal calibration was carried out using narrow molecular weight distribution polystyrene standards from Polymer Laboratories with Ionol (4-(2,6,6-trimethyl-2-cyclohexen-1-yl)-3-buten-2-ol)[6] added as the flow marker.

Ethylene Polymerization Experiments. Ethylene polymerizations were carried out on a high-vacuum line (10^{-5} Torr) in 250 mL round-bottom three-neck Morton flasks equipped with large magnetic stirring bars and thermocouple probes. In a typical experiment, dry toluene (100 mL) was vacuum-transferred into the flask from Na/K, presaturated under 1.0 atm of rigorously purified ethylene (pressure control using a mercury bubbler), and equilibrated at the desired reaction temperature using an external bath. The catalytically active species was freshly generated by mixing measured amounts of precatalyst and cocatalyst in a septum-capped vial in the glovebox, to which 2 mL of dry 1,2-difluorobezene was added. (In the MAO experiments, the mixture was stirred vigorously at room temperature for 30 min before use.) The catalyst solution was then removed from the glovebox and quickly injected into the rapidly stirring flask using a gastight syringe equipped with a spraying needle. The temperature of the toluene solution in representative polymerization experiments was monitored using a thermocouple (OMEGA Type K thermocouple with a model HH21 microprocessor thermometer). The exothermic temperature rise was invariably less than 3 °C during these polymerizations. After a measured time interval, the polymerization was quenched by the addition of 15 mL of 2% acidified methanol. The solution was then reduced to ~20 mL by removing the volatiles under vacuum. Another 100 mL of methanol was then added, and the polymer was collected by filtration, washed with methanol, and dried on the high-vacuum line overnight to a constant weight.

Ethylene Copolymerization Experiments. The procedure for ethylene + 1-hexene copolymerizations was similar to that for the 1.0 atm of ethylene polymerizations described above. A measured quantity of 1-hexene was vacuum-transferred into a graduated flask. The required amount of 1-hexene (10 mL) was then vacuum-transferred into the polymerization flask containing 100 mL of toluene. The mixture was next presaturated under 1.0 atm of ethylene. The procedures for catalyst preparation, injection into the polymerization flask, and copolymer workup are same as described above.

Synthesis of Bis(3-indenyl)methane (Modification of Published Procedure).[7] Formalin (37% solution, 4.2 g, 52.0 mmol) was added to a mixture of indene (15.0 g, 104.1 mmol) and sodium ethoxide (2.25 g, 33.0 mmol) in DMF (150 mL). The reaction mixture was stirred at room temperature for 24 h, and then aqueous HCl solution (1.0 M, 100 mL) was added. The mixture was next extracted with CH_2Cl_2 (2 × 50 mL). The organic phases were combined, washed with brine and then with water, dried over $MgSO_4$, and filtered, and the filtrate was concentrated to yield a brown oil. The resulting dark brown oil was fractionally distilled to give bis(3-indenyl)-methane (7.1 g, 56% yield) as a pale-yellow oil (bp 180−182 °C/0.1 mmHg). The product can be recrystallized from ethanol to give white needles. Spectroscopic and analytical data are consistent with the literature[5] and are as follows. MS (EI): *m/e* 244 (M+, 100%) ^{1}H NMR (C_6D_6, 23 °C, 499.579 MHz): δ 7.34 (d, 2 H, $^3J_{H-H}$ = 6 Hz, Ind, C_6H_4), 7.31 (d, 2 H,$^3J_{H-H}$ = 6 Hz, Ind, C_6H_4), 7.24 (t, 2H, $^3J_{H-H}$ = 6 Hz, Ind, C_6H_4), 7.16 (t, 2 H,$^3J_{H-H}$ = 6 Hz, Ind, C_6H_4), 6.02 (s, 2 H, Ind, C_5H), 3.69 (s, 4 H, CH_2CH_2), 3.05 (s, 4 H). ^{13}C NMR (C_6D_6, 23 °C, 125.633 MHz): δ 146.01 (Ind), 145.07 (Ind), 142.39 (Ind), 130.36 (Ind), 126.80 (Ind), 125.37 (Ind), 124.39 (Ind), 120.16(Ind), 38.30 (Ind), 27.50 (CH_2).

Synthesis of (μ-CH_2-3,3′)[1-(Me_2SiCl)indenyl]$_2$. In a 250 mL flask, 1,2-bis(3-indenyl)methane (7.0 g, 28.7 mmol) was dissolved in 150 mL of dry THF, and the solution was cooled to −78 °C. Next, 39.5 mL of ^{n}BuLi (1.6 M in hexanes, 63.1 mmol) was added dropwise by syringe with stirring. The solution became light brown and was allowed to warm slowly to room temperature overnight. The solution was then slowly added to a solution of Me_2SiCl_2 (16 mL) in 100 mL of THF at −78 °C, and the reaction mixture was allowed to warm slowly to room temperature with stirring. All the volatiles were next removed under vacuum, and the product was extracted with pentane. An oily product was obtained after filtration and removal of the pentane in vacuo. Yield: 9.0 g (75%). The product consists of two diastereomers [(*RR*, *SS*) and (*RS*, *SR*)] in a 1:1 ratio and was used without further purification in the next step. Spectroscopic and analytical data for the mixture are as follows. ^{1}H NMR (C_6D_6, 23 °C, 499.579 MHz): δ 7.519 (d, 2 H, $^3J_{H-H}$ = 7.0 Hz, Ind, C_6H_4), 7.383 (d, 2 H, $^3J_{H-H}$ = 7.5 Hz, Ind, C_6H_4), 7.212 (t, 2 H, $^3J_{H-H}$ = 7.0 Hz, Ind, C_6H_4), 7.141-(t, 2 H, $^3J_{H-H}$ = 6.5 Hz, Ind, C_6H_4), 6.248 (s, 2 H, Ind, C_5H_2), 6.231 (s, 2 H, Ind, C_5H_2), 3.824 (s, 2 H, CH_2), 3.781 (s, 2 H, CH_2), 3.424 (s, 2 H, Ind, C_5H_2), 3.409 (s, 2 H, Ind, C_5H_2), 0.011 (s, 6 H, Si*Me*$_2$), −0.010 (s, 6 H, Si*Me*$_2$), −0.021 (s, 6 H, Si*Me*$_2$), −0.047 (s, 6 H, Si*Me*$_2$). ^{13}C NMR (C_6D_6, 23 °C, 125.633 MHz): δ 145.243 (Ind), 144.470 (s, Ind), 142.044 (s, Ind), 130.249 (Ind), 126.303 (Ind), 125.325 (Ind), 124.156 (Ind), 120.651 (Ind), 46.260 (Ind), 27.722 (CH_2), −0.244 (q, $^1J_{C-H}$ = 121.6 Hz, $SiMe_2$), 0.523 ($SiMe_2$).

Synthesis of (μ-CH_2-3,3′)[1-(Me_2SiNH^tBu)indenyl]$_2$ (MBICGCH$_2$). The reagent (μ-CH_2-3,3′)[1-(Me_2SiCl)indenyl]$_2$ (9.00 g, 21.4 mmol) was dissolved in THF (150 mL) in a 250 mL flask, and the solution was cooled to 0 °C. Next, ^{t}BuNH$_2$ (13.0 mL, 123.5 mmol) was added dropwise by syringe with

stirring. A white precipitate formed immediately. The solution was stirred at room temperature overnight. All the volatiles were then removed under vacuum, and the product was extracted with pentane. An orange oily product was obtained after filtration and removal of the pentane in vacuo. The product consists of two diastereomers [(*RR*, *SS*) and (*RS*, *SR*)] in a ~1:1 ratio. The product was used to synthesize bimetallic complexes without further purification. Yield: 8.2 (76.3%). Spectroscopic and analytical data for the mixture are as follows. ^{1}H NMR (C_6D_6, 23 °C, 499.579 MHz): δ 7.640 (d, 4 H, $^3J_{H-H}$ = 7.0 Hz, Ind, C_6H_4), 7.578 (d, 4 H, $^3J_{H-H}$ = 7.5 Hz, Ind, C_6H_4), 7.307 (t, 4 H, $^3J_{H-H}$ = 7.5 Hz, Ind, C_6H_4), 7.257(t, 4 H, $^3J_{H-H}$ = 7.5 Hz, Ind, C_6H_4), 6.462 (s, 4 H, Ind, C_5H_2), 4.018 (4H, CH_2), 3.470 (s, 4 H, Ind, C_5H_2), 1.067 (s, 32H, $NCMe_3$), 0.502 (br, 4 H, NH), −0.001 (s, 6 H, Si*Me*$_2$), −0.015 (s, 6 H, Si*Me*$_2$), −0.049 (s, 6 H, Si*Me*$_2$), −0.075 (s, 6 H, Si*Me*$_2$) ^{13}C NMR (C_6D_6, 23 °C, 125.633 MHz): δ 146.926 (s, Ind), 145.576 (s, Ind), 140.094 (s, Ind), 132.965 (s, Ind), 125.340 (Ind), 124.408 (Ind), 123.870 (Ind), 120.427 (Ind), 49.896 (s, N*C*Me$_3$), 47.486 (Ind), 34.195), 34.237 (NC*Me*$_3$), 27.800 (CH_2), 0.801 ($SiMe_2$), −0.170 ($SiMe_2$).

Synthesis of MBICGC[Zr(NMe$_2$)$_2$]$_2$. MBICGCH$_2$ (μ-CH_2-3,3′)[1-(Me_2SiNH^tBu)indenyl]$_2$ (prepared by procedure above, 5.00 g, 9.96 mmol) was dissolved in 35 mL of pentane. A solution of $Zr(NMe_2)_4$ (5.34 g, 19.9 mmol) in 100 mL of toluene was then added, and the solution was refluxed at 110 °C for 8 h under slow but constant N_2 purge to remove evolved $HNMe_2$. Yield: 5.6 g (66%). Spectroscopic and analytical data: ^{1}H NMR (C_6D_6, 23 °C, 499.579 MHz): δ 7.470−7.453 (m, 2 H, Ind, C_6H_4), 7.332−7.315 (m, 2 H, Ind, C_6H_4), 7.021−6.802 (m, 4 H, Ind, C_6H_4), 6.727 (s, 2 H, Ind, C_5H), 6.583 (s, 2 H, Ind, C_5H), 4.764 (br, s, 2 H, CH_2), 3.033 (s, 6 H, $ZrNMe_2$), 3.021 (s, 6 H, $ZrNMe_2$), 2.249 (s, 6 H, $ZrNMe_2$), 2.232 (s, 6 H, $ZrNMe_2$), 1.256 (s, 9 H, $NCMe_3$), 1.237 (s, 9 H, $NCMe_3$), 0.817 (s, 6 H, Si*Me*$_2$), 0.806 (s, 6 H, Si*Me*$_2$), 0.661 (s, 6 H, Si*Me*$_2$), 0.526 (s, 6 H, Si*Me*$_2$). ^{13}C NMR (C_6D_6, 23 °C, 499.579 MHz): δ 133.611 (Ind), 129.680 (Ind), 128.911 (Ind), 125.812 (Ind), 124.961 (Ind), 124.702 (Ind), 124.129 (Ind), 122.702 (Ind), 122.299 (Ind), 120.740 (Ind), 91.525 (Ind), 91.433 (Ind), 56.906 (N*C*Me$_3$), 45.200 ($ZrNMe_2$), 45.127 ($ZrNMe_2$), 42.960 ($ZrNMe_2$), 42.836 ($ZrNMe_2$), 35.026 (NC*Me*$_3$), 26.925 (−CH_2−), 6.175 ($SiMe_2$), 3.997 ($SiMe_2$).

Synthesis of MBICGC(ZrMe$_2$)$_2$ (C1-Zr$_2$). MBICGC[Zr-(NMe$_2$)$_2$]$_2$ (**1**, 800 mg, 0.92 mmol) was dissolved with 50 mL of pentane. A solution of $AlMe_3$ (5.0 mL, 2.0 M in hexanes) was added slowly by syringe at 25 °C. The solution first became yellow and then cloudy during the addition. The solution was stirred at 25 °C for an additional 12 h. All the volatiles were then removed in vacuo, and the white solid product was washed with pentane. The product consists of two diastereomers (*RS*, *SR*) and (*SS*, *RR*) (1:1.1 or 1.1:1 ratio) as indicated by NMR spectra. Yield: 587 mg (84%). Spectroscopic and analytical data for C_1-Zr_2: ^{1}H NMR (C_6D_6, 23 °C, 499.579 MHz): δ 7.579 (d, 2 H, $^3J_{H-H}$ = 8.0 Hz, Ind, C_6H_4), 7.452 (d, 2 H, $^3J_{H-H}$ = 7.0 Hz, Ind, C_6H_4), 7.044 (dd, 2 H, $^3J_{H-H}$ = 7.0 Hz, $^3J_{H-H}$ = 6.7 Hz, Ind, C_6H_4), 6.956 (dd, 2 H, $^3J_{H-H}$ = 7.0 Hz, Ind, C_6H_4), 6.458 (s, 2 H, Ind, C_5H), 3.238 (br, s, 4 H, CH_2-CH_2), 1.360 (s, 9 H, $NCMe_3$), 1.317 (s, 9 H, $NCMe_3$),0.581 (s, 6 H, $SiMe_2$), 0.414 (s, 6 H, $SiMe_2$), 0.237 (s, 6 H, $ZrMe_2$), −0.627 (s, 6 H, $ZrMe_2$). ^{13}C NMR (C_6D_6): δ 133.936 (Ind), 130.257 (Ind), 126.473 (Ind), 125.862 (Ind), 125.491 (Ind), 124.121 (Ind), 123.943 (Ind), 122.098 (Ind), 86.402 (Ind), 55.900 (N*C*Me$_3$), 41.482 ($ZrMe_2$), 39.765($ZrMe_2$), 34.670 (NC*Me*$_3$), 27.741 (−CH_2−), 4.724 ($SiMe_2$), 2.999 ($SiMe_2$). Anal. Calcd for $C_{35}H_{54}N_2Si_2Zr_2$: C, 56.72; H, 7.29; N, 3.78. Found: C, 56.11; H, 7.07; N, 3.72.

Synthesis of MBICGC[ZrCl$_2$]$_2$ (C1-Zr$_2$Cl$_4$). MBICGC[Zr-(NMe$_2$)$_2$]$_2$ (**1**, 800 mg, 0.93 mmol) was dissolved in 50 mL of toluene. Me_3SiCl (10 mL) was then added by syringe with stirring at 25 °C. The solution was stirred overnight. All the volatiles were then removed in vacuo, and the white solid product was washed with pentane three times. The product consists of two diastereomers (*RS*, *SR*) and (*SS*, *RR*) in a 1:1.3 or 1.3:1 ratio as indicated by ^{1}H NMR spectra. Yield: 680 mg (89%). Spectroscopic and analytical data: ^{1}H NMR (C_6D_6, 23 °C, 499.579 MHz): δ 7.715−7.566 (m, 4 H, Ind, C_6H_4), 7.534−7.402 (m, 4 H, Ind, C_6H_4), 7.116−7.017 (m, 4 H, Ind, C_6H_4), 6.999−6.886 (m, 4 H, Ind, C_6H_4), 6.685 (s, 2 H, Ind, C_5H), 6.482 (s, 2 H, Ind, C_5H), 4.837 (m, 2 H, CH_2), 1.273 (s, 9 H, $NCMe_3$), 1.256 (s, 9 H, $NCMe_3$), 0.598 (s, 6 H, $SiMe_2$), 0.543 (s, 6 H, $SiMe_2$), 0.354 (s, 6 H, $SiMe_2$), 0.313 (s, 6 H, $SiMe_2$). ^{13}C NMR (C_6D_6): δ 133.385 (Ind), 131.726 (Ind), 131.500 (Ind), 126.871 (Ind), 126.550 (Ind), 126.160 (Ind), 124.047 (Ind), 123.594 (Ind), 117.122 (Ind), 116.507 (Ind), 92.280 (Ind), 57.717 (N*C*Me$_3$), 32.808 (NC*Me*$_3$), 32.379 (NC*Me*$_3$), 27.121 (CH_2), 26.050 (CH_2), 3.705 ($SiMe_2$), 3.635 ($SiMe_2$), 1.682 ($SiMe_2$), 1.407 ($SiMe_2$). Anal. Calcd for $C_{31}H_{42}N_2Si_2Zr_2Cl_4$: C, 45.23; H, 5.11; N, 3.40. Found: C, 44.41; H, 4.91; N, 3.21.

Synthesis of (1)-Naphthylindene (Modification of Literature Procedure).[8] The reagent 1-bromonaphthalene (15.7 g, 75.8 mmol) in 50 mL of diethyl ether, was added from a pressure-equalizing dropping funnel to Mg turnings (1.01 g, 45.8 mmol) suspended in 200 mL of diethyl ether. After all the Mg had been consumed, 1-indanone (10.00 g, 75.6 mmol) in 100 mL of diethyl ether was slowly added dropwise via a cannula, at 0 °C. The white suspension that formed was stirred overnight at room temperature, and the reaction was then terminated by the addition of 50 mL of a saturated aqueous NH_4Cl solution at 0 °C. The diethyl ether layer was next separated, dried over $MgSO_4$, and filtered, and the solvent was removed on a rotary evaporator to yield a yellow solid. This was taken up in 100 mL of toluene together with 1.0 g of *p*-toluenesulfonic acid and allowed to undergo reaction for 4 h. The acid was then neutralized by addition of 50 mL of saturated aqueous Na_2CO_3 solution. The organic material was extracted into diethyl ether, separated, dried over $MgSO_4$, and filtered, and the solvent was removed at the rotary evaporator to yield a yellow oil. Yield: 9.7 g (51%). ^{1}H NMR (23 °C, 499.551 MHz, $CDCl_3$): δ 7.85−7.89 (m, 3H, arom H), 7.07−7.57 (m, 8H, arom H), 6.62 (d, ^3J = 7 Hz, 1H, 2-CH), 3.61 (d, ^3J = 7.9 Hz, 2H, 1-CH_2). ^{13} C NMR (125.63 MHz, $CDCl_3$) δ 145.91, 144.33, 144.14, 134.10, 133.22, 132.07, 128.44, 128.05, 126.73, 126.45, 126.36, 126.17, 126.03, 125.94, 125.04, 124.08 (arom C), 121.87 (C-3), 121.04 (C-2), 38.77 (C1). MS (EI): *m/e* 242 (M+, 100%).

Synthesis of Dimethyl [3-(1)-naphthyl-1-indenyl]chlorosilane. To 9.7 g (40 mmol) of 1-naphthylindene dissolved in 100 mL of pentane was added ^{n}BuLi (2.5 M in hexanes, 20 mL, 50 mmol) with stirring at −78 °C, and after slowly warming, the solution was stirred at room temperature overnight. The product was next washed with pentane twice and then redisolved in 100 mL of THF. In a separate flask, 20 mL of Me_2SiCl_2 was dissolved in 50 mL of THF and cooled to 0 °C. The 1-naphthylindenyllithium solution was next added slowly to the silane solution with stirring. The reaction mixture was allowed to stir at room temperature overnight. The crude dimethyl[3-(1)-naphthyl-1-indenyl]chlorosilane was used directly for the subsequent reaction following removal of excess Me_2SiCl_2 and solvent in vacuo. Spectroscopic data for dimethyl-[3-(1)-naphthyl-1-indenyl]chlorosilane are as follows. ^{1}H NMR (23 °C, $CDCl_3$, 499.903 MHz): δ 7.903−7.961 (m, 3 H, arom H), 7.202−7.723 (m, 8 H, arom H), 6.793 (s, 1 H, Ind, C_5H_2), 4.000 (s, 1 H, C_5H_2), 3.781 (s, 1 H, C_5H_2), 0.424 (s, 3 H, $SiMe_2$), 0.394 (s, 3 H, $SiMe_2$). ^{13}C NMR (23 °C, $CDCl_3$, 125.626 MHz): δ 145.191, 144.011, 143.443, 134.030, 132.746, 132.130, 128.594, 128.339, 127.082, 126.474, 126.111, 126.096, 126.037, 125.770, 124.981, 123.755, 121.561, 116.601 (arom C), 47.127 (CH, Ind), 0.698($SiMe_2$), 0.393 ($SiMe_2$).

Synthesis of (1-Me$_2$SiNH^{t}Bu)[3-(1)-naphthyl]indene. The crude dimethyl [3-(1)-naphthyl-1-indenyl]chlorosilane was redissolved in THF (100 mL) in a 250 mL flask, and the solution was cooled to 0 °C. Next, ^{t}BuNH$_2$ (20.7 mL, 0.200 mol) was added dropwise by syringe with stirring. The solution turned cloudy immediately and was stirred at room temperature overnight. All volatiles were then removed under vacuum, and the product was extracted with pentane. An orange oily product was obtained after filtration and pentane removal in vacuo. The product was used without further purification. Yield: 9.3 g (63%). Spectroscopic data for the ligand are as follows: ^{1}H NMR (23 °C, $CDCl_3$, 499.551 MHz):

δ 7.929−8.020 (3 H, arom. H), 7.221−7.703(d, 1 H, $^3J_{H-H}$ = 7 Hz, Ind, C_6H_4), 7.220−7.345 (m, 8 H arom. H), 6.346 (s, 1 H C_5H_2), 3.885 (1 H C_5H_2, C_5H_2), 3.794 (1 H C_5H_2), 1.297 (s, 9H, $NCMe_3$), 0.807 (br, s, 1 H, NH), 0.141 (d, 3 H, $SiMe_2$), 0.121 (s, 3 H, $SiMe_2$). ^{13}C NMR ($CDCl_3$ 125.626 MHz): δ 145.872, 145.036, 141.322, 136.115, 135.225, 134.072, 132.386, 128.517, 127.906, 127.058, 126.811, 126.026, 125.906, 125.809, 124.904, 124.064, 123.426, 121.054 (arom C), 68.250 (CH, Ind), 48.647 (s, N*C*Me_3), 34.194 ($NCMe_3$), 0.362 ($SiMe_2$), −0.203 ($SiMe_2$).

Synthesis of {1-Me_2Si[3-(1)-naphthyl-indenyl](^{t}BuN)}-$ZrCl_2$ (N-$ZrCl_2$). The complex{1-Me_2Si[3-(1)-naphthylindenyl]-(^{t}BuN)}$Zr(NMe_2)_2$ (2.40 g, 4.38 mmol) was dissolved in 50 mL of pentane in a 250 mL flask. A solution of Me_3SiCl (18.0 mL) was then added by syringe at room temperature. The solution turned cloudy immediately after the addition. The solution was then stirred at room temperature overnight, and all volatiles were removed in vacuo. The yellow solid product was washed with pentane at room temperature. Yield: 2.3 g (97%). Spectroscopic and analytical data are as follows. ^{1}H NMR (C_6D_6, 23 °C, 499.551 MHz): δ 7.745−8.023 (m, 6 H, arom H), 7.014−7.349 (m, 5 H, arom H), 6.830 (s, 1 H, Ind, C_5H), 1.268 (s, 9 H, $NCMe_3$), 0.680 (s, 3 H, $SiMe_2$), 0.366 (s, 3 H, $SiMe_2$). ^{13}C NMR (C_6D_6, 23 °C, 125.626 MHz): δ 135.749, 135.161, 129.937, 129.539, 129.446, 129.231, 129.110, 128.992, 128.893, 128.687, 127.754, 126.986, 126.745, 126.660, 126.412, 126.124, 125.994, 125.395, 95.452 (arom C), 57.242 (s, N*C*Me_3), 32.828 (NC*Me*$_3$), 3.955 ($SiMe_2$), 1.418 ($SiMe_2$). Anal. Calcd for $C_{25}H_{27}Cl_2NSiZr$: C, 56.50; H, 5.08; N, 2.64. Found: C, 55.79; H, 5.59; N, 2.45.

Synthesis of of {1-Me_2Si[3-(1)-naphthyl-indenyl](^{t}BuN)}-$ZrMe_2$ (N-Zr_1). The complex {1-Me_2Si[3-(1)-naphthylindenyl]-(^{t}BuN)}$ZrCl_2$ (300 mg, 0.56 mmol) was dissolved in 30 mL of ethyl ether in a 100 mL flask. A solution of MeLi (0.7 mL, 1.6 M in ethyl ether) was added by syringe with stirring at room temperature. The yellow solution became colorless and then cloudy immediately after the addition. The solution was stirred at room temperature for another 2 h. All the volatiles were then removed under vacuum, and the yellow solid product was extracted with pentane, filtered, and recrystallized from pentane at −78 °C. Yield: 0.165 g (60%). Spectroscopic and analytical data for N-Zr_1 are as follows: ^{1}H NMR (C_6D_6, 23 °C, 499.903 MHz): δ 7.640−8.267 (m, 4H, arom H), 6.971−7.374 (m, 7 H, arom H), 6.786 (s, 1 H, Ind, C_5H), 1.330 (s, 9 H, $NCMe_3$), 0.709 (s, 3 H, $SiMe_2$), 0.429 (s, 3 H, $SiMe_2$), 0.138 (s, 3 H, Zr-Me), −0.459 (s, 3 H, Zr-Me). ^{13}C NMR (C_6D_6, 125.626 MHz): δ 135.455, 134.211, 133.987, 133.150, 131.380, 129.602, 129.254, 128.917, 127.138, 126.936, 126.789, 126.716, 126.615, 126.430, 126.252, 126.178, 125.965, 125.180, 89.610 (arom C), 55.650 (N*C*Me_3), 40.987 (Zr−Me), 40.070 (Zr−Me), 34.027 (NC*Me*$_3$), 4.501 ($SiMe_2$), 2.397 ($SiMe_2$). Anal. Calcd for $C_{27}H_{33}NSiZr$: C, 66.12; H, 6.73; N, 2.86. Found: C, 65.49; H, 6.75; N, 2.60.

X-ray Crystal Structure Determination of MBICGC-$[Zr(NMe_2)_2]_2$ (1) and {1-Me_2Si[3-(1)-naphthyl-indenyl]-(^{t}BuN)}$ZrCl_2$ (2). Suitable crystals of **1** and **2** for diffraction studies were grown by slowly cooling of concentrated toluene solutions from room temperature to −30 °C. Inside the glovebox, the crystals were placed on a glass slide and covered with Infineum V8512 oil. The crystals were then removed from the box, and a suitable crystal was chosen under a microscope using plane-polarized light. The crystal was mounted on a glass fiber and transferred to a Bruker SMART 1000 CCD area detector diffractometer having a nitrogen cold stream at 153-(2) K. Twenty frames (20 s exposures, 0.3° slices) were collected in three areas of space to determine the orientation matrix. The parameters for data collection were determined by the peak intensities and widths from the 60 frames used to determine the orientation matrix. The faces of the crystal were next indexed, and data collection was begun. After data collection, the frames were integrated, the initial crystal structure was solved by direct methods, the structure solution was expanded through successive least-squares cycles, absorption corrections were applied, and the final solution was determined. Crystal, data collection, and refinement parameters are given in Tables S1 and S2 in the Supporting Information.

Results

The goal of this study was to investigate metal−metal proximity and cocatalyst effects on ethylene homopolymerization and ethylene + α-olefin copolymerizations in bimetallic coordinatively "open" CGCZr ("constrained geometry catalyst") core structures and to study ligand steric as well as polymerization solvent polarity effects on the polymerization systems. Thus, the new methylene-bridged bimetallic "constrained geometry" catalysts (CGC) C1-Zr_2 and the naphthyl-substituted monometallic CGC complex N-Zr_1 were synthesized for this purpose. It will be seen that the effect of increasing achievable catalyst metal−metal proximity is to significantly enhance polyolefin product molecular weight and comonomer enchainment selectivity. Moreover, it is found that the cocatalyst/counteranion and polymerization solvent significantly influences chain transfer rate, polymerization activity, and comonomer enchainment selectivity, while ancillary ligand substituent steric hindrance alone in the catalyst structure does not exert a major influence.

Synthesis. I. Bimetallic Metallocene Precatalyst MBICGC$(ZrMe_2)_2$ (C1-Zr_2). The ligand (μ-CH_2-3,3′)[1-(Me_2SiNH^tBu)indenyl]$_2$ (MBICGCH_2), synthesized according to a modification of the literature procedure,[3f] consists of two diastereomers (*RR*, *SS*) and (*RS*, *SR*) in an approximately 1:1 ratio as indicated by ^{1}H and ^{13}C NMR spectra. Similar to the synthesis of the −CH_2-CH_2− bridged analogue, bimetallic constrained geometry complex MBICGC$(ZrMe_2)_2$ (C1-Zr_2) was synthesized by the methodology outlined in Scheme 1. Thus, the bimetallic amido complex MBICGC$[Zr(NMe_2)_2]_2$ (**1**) was synthesized via the protodeaminative reaction of the free (3,3′-CH_2)[1-Me_2SiNH^tBuInd]$_2$ (MBICGCH_2) ligand with $Zr(NMe_2)_4$ in refluxing toluene, driven by continuous removal of the volatile $HNMe_2$ coproduct. The course of the reaction is similar to that of the −CH_2-CH_2− bridged analogue except that longer reaction times are required in the metalation step, presumably due to steric constraints. The product is formed as two diastereomers (*RS*, *SR*) and (*SS*, *RR*) in a 1:1.3 or 1.3:1 ratio as indicated by ^{1}H NMR spectroscopy. Bimetallic amido complex **1** was characterized by standard spectroscopic and analytical techniques and one diastereomer (*SS*, *RR*) by X-ray diffraction (see below). Reaction of complex **1** with excess $AlMe_3$ at room temperature cleanly forms the bimetallic metallocene dimethyl complex C1-Zr_2 (Scheme 1), which can be purified by

Scheme 1. Synthetic Routes to Complexes C1-Zr_2 and C1-Zr_2Cl_4

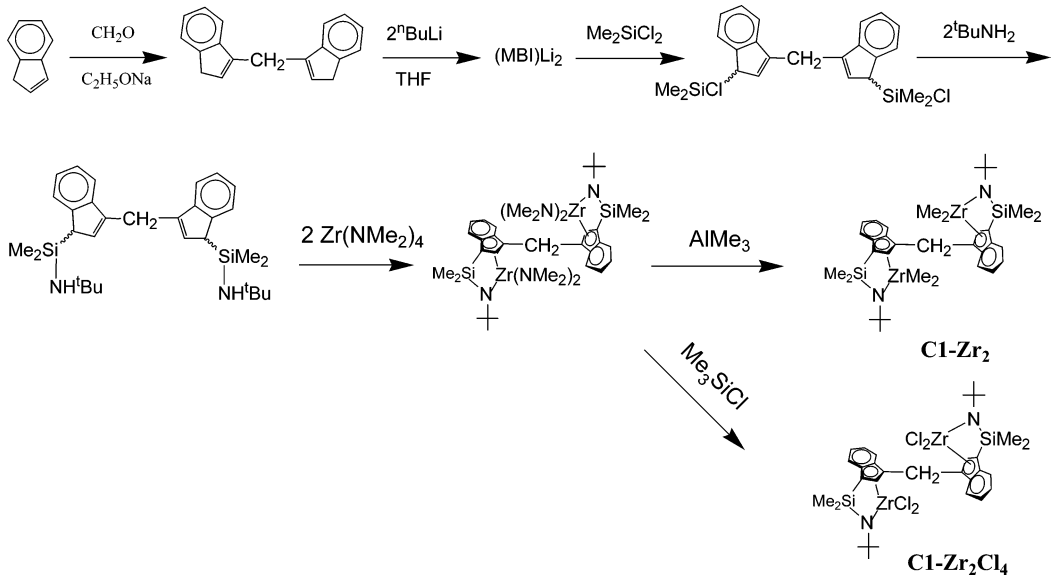

Scheme 2. Synthetic Route to Complexes N-Zr_1 and N-Zr_1Cl_2

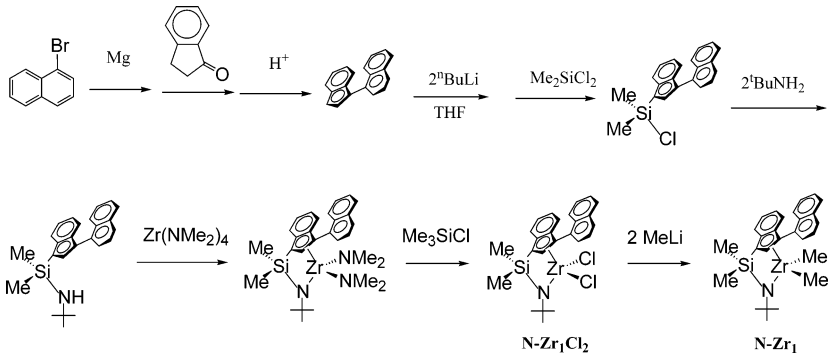

repeated washing with pentane and has been characterized spectroscopically and analytically. Both (*RS*, *SR*) and (*SS*, *RR*) diastereomers (1:1.1 or 1.1:1 ratio) are present in the product.

II. Synthesis of of {1-Me_2Si[3-(1)-naphthylindenyl]-(^{t}BuN)}$ZrMe_2$ (N-Zr_1). The monometallic metallocene complex {1-Me_2Si[3-(1)-naphthylindenyl](^{t}BuN)}$ZrMe_2$ (N-Zr_1) was synthesized as a control for studies of catalyst structure steric effects on ethylene polymerization. Here a bulky, relatively rigid ligand substituent is placed in closed proximity to the polymerization zone. The ligand (1-Me_2SiNH^{t}Bu)[3-(1)-naphthyl]indene was synthesized from 1-naphthylindene, which was in turn prepared according to the literature procedure.[8] The monometallic CGC complex was then synthesized via methodology similar to that for the ethyl-substituted complex [1-Me_2Si(3-ethylindenyl)(^{t}BuN)]$ZrMe_2$ (Zr_1; Scheme 2). Thus, the monometallic amido complex {1-Me_2Si[3-(1)-naphthylindenyl](^{t}BuN)}$Zr(NMe_2)_2$ (**2**) was synthesized via the reaction of the free (1-Me_2SiNH^t-Bu)[3-(1)-naphthyl]indene ligand with $Zr(NMe_2)_4$ in the refluxing toluene, using continuous removal of the evolved $HNMe_2$. The reaction of **2** with excess Me_3SiCl at room temperature then cleanly affords the dichloro complex {1-Me_2Si[3-(1)-naphthyl-indenyl](^{t}BuN)}$ZrCl_2$ (**3**), and subsequent reaction with MeLi affords the metallocene dimethyl complex {1-Me_2Si[3-(1)-naphthyl-indenyl](^{t}BuN)}$ZrMe_2$ (N-Zr_1). Monometallic complexes **3** and N-Zr_1 were characterized by standard spectroscopic and analytical techniques and **3** by X-ray diffraction (vide infra).

Table 1. Selected Bond Distances (Å) and Angles (deg) for MBICGC[$Zr(NM_2)_2]_2$ (1)

Bond Distances			
Zr(1)−N(1)	2.0980(16)	Zr(1)−N(2)	2.0665(16)
Zr(1)−N(3)	2.0428(16)	Zr(1)−C(1)	2.4725(18)
Zr(1)−C(2)	2.5482(18)	Zr(1)−C(3)	2.6259(18)
Zr(1)−C(4)	2.6267(18)	Zr(1)−C(9)	2.5447(18)
C(3)−C(21)	1.509(2)	N(2)−C(16)	1.453 (3)
Si(1)−C(11)	1.858(2)	Si(1)−N(1)	1.7355(17)
Angles			
N(3)−Zr(1)−N(2)	105.12(7)	N(3)−Zr(1)−N(1)	103.92(7)
N(2)−Zr(1)−N(1)	108.90(6)	N(1)−Zr(1)−C(1)	70.93(6)
N(1)−Si(1)−C(1)	95.49(8)	N(4)−Si(2)−Zr(2)	41.96(6)
N(1)−Si(1)−C(10)	109.49(9)	C(16)−N(2)−C(17)	109.54(17)
C(4)−C(3)−C(21)	126.78(16)	C(12)−N(1)−Zr(1)	127.66(12)
C(3)−C(21)−C(24)	113.10(15)	C(16)−N(2)−Zr(1)	124.25(14)
C(16)−N(2)−Zr(1)	124.25(14)	C(2)−C(1)−Si(1)	118.85(13)

Crystal Structures of Complexes MBICGC[Zr-($NM_2)_2]_2$ (1) (Comparison with EBICGC[Zr-($NM_2)_2]_2$) and Monometallic Complex {1-Me_2Si[3-(1)-naphthylindenyl](^{t}BuN)}$ZrCl_2$ (N-Zr_1Cl_2). I. Bimetallic Complex Comparison. A summary of crystal structure data for methylene-bridged binuclear bis(dimethylamido) complex MBICGC[$Zr(NMe_2)_2]_2$ (**1**) is presented in Table S1 of the Supporting Information. Selected bond distances and angles for **1** and ethylene-bridged EBICGC[$Zr(NMe_2)_2]_2$[3f] are summarized in Tables 1 and 2. Figure 1 shows the solid-state structures of complexes **1** and EBICGC[$Zr(NMe_2)_2]_2$. It can be seen that the molecular structure of **1** is asymmetric, different from that of EBICGC[$Zr(NMe_2)_2]_2$, which has an

Table 2. Selected Bond Distances (Å) and Angles (deg) for EBICGC[Zr(NM$_2$)$_2$]$_2$

Bond Distances			
Zr(1)−N(1)	2.133(2)	Zr(1)−N(2)	2.065(2)
Zr(1)−N(3)	2.049(2)	Zr(1)−C(1)	2.533(2)
Zr(1)−C(2)	2.491(2)	Zr(1)−C(3)	2.604(2)
Zr(1)−C(8)	2.673(2)	Zr(1)−C(9)	2.598(1)
N(1)−C(12)	1.496(3)	N(2)−C(16)	1.460(5)
Si(1)−C(2)	1.884(2)	Si(1)−N(1)	1.734(2)
Angles			
N(3)−Zr(1)−N(2)	106.08(11)	N(3)−Zr(1)−N(1)	108.11(9)
N(2)−Zr(1)−N(1)	106.08(10)	N(1)−Si(1)−C(2)	95.67(10)
N(1)−Si(1)−C(11)	116.81(14)	C(2)−Si(1)−C(11)	108.18(13)
N(1)−Si(1)−C(10)	115.33(13)	C(12)−N(1)−Si(1)	127.6(2)
C(12)−N(1)−Zr(1)	126.6(2)	Si(1)−N(1)−Zr(1)	105.25(10)
C(16)−N(2)−C(17)	109.5(3)	C(16)−N(2)−Zr(1)	125.2(2)
C(17)−N(2)−Zr(1)	124.9(2)	C(18)−N(3)−C(19)	111.2(3)
C(18)−N(3)−Zr(1)	116.2(2)	C(19)−N(3)−Zr(1)	131.2(2)
C(1)−C(2)−C(3)	104.8(2)	C(1)−C(2)−Si(1)	120.6(2)
C(3)−C(2)−Si(1)	127.0(2)	C(1)−C(9)−C(8)	106.5(2)
C(1)−C(9)−C(20)	128.2(2)	C(8)−C(9)−C(20)	124.8(2)

inversion center (Figure 1B). The C(3)−C(21) bridge atom−indenyl ligand bond length is 1.509(2) Å in MBICGC[Zr(NMe$_2$)$_2$]$_2$, shorter than the corresponding C(9)−C(20) bond length (1.518(2) Å) in the EBICGC-[Zr(NMe$_2$)$_2$]$_2$ analogue, reflecting the influence of two adjacent aromatic rings on bridging geometry in the former case. It can also be seen that the shorter methylene bridge forces the two indenyl rings into a twisted conformation with a C(4)−C(3)−C(21)−C(24) dihedral angle of 56.1(2)°. This brings the two Zr atoms to the same side of the molecule, significantly different from the orientation in the crystal structure of EBICGC-[Zr(NMe$_2$)$_2$]$_2$, in which the two Zr centers are located on opposite sides of the molecule in the solid state. The Zr−Zr distance in MBICGC[Zr(NMe$_2$)$_2$]$_2$ is 7.392(3) Å, ∼1.28 Å shorter than that in the EBICGC[Zr(NMe$_2$)$_2$]$_2$, where this distance is 8.671(3) Å. The N(1)−Zr(1) ring centroid angle in MBICGC[Zr(NMe$_2$)$_2$]$_2$ is 100.67(6)°, showing that the Me$_2$Si⟨ bridge forces the indenyl plane to tilt, rendering the structure more open. The sum of the bond angles around nitrogen atom N(1) in complex

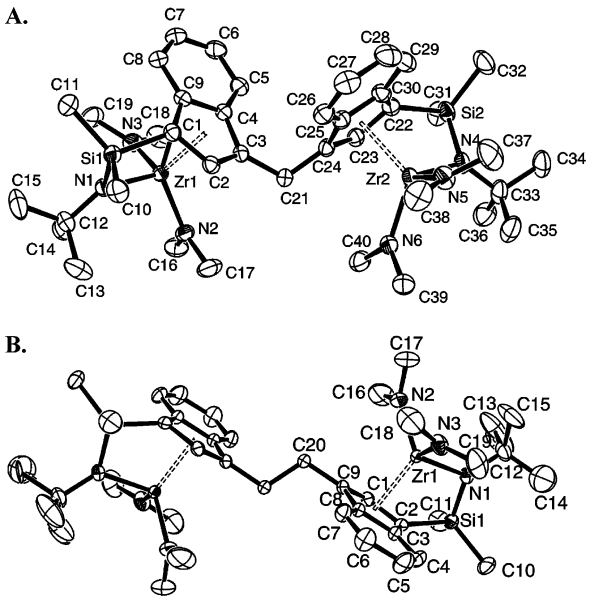

Figure 1. Molecular structure and atom numbering scheme for ligand methylene-bridged MBICGC[Zr(NMe$_2$)$_2$]$_2$ (A) and for ligand ethylene-bridged EBICGC[Zr(NMe$_2$)$_2$]$_2$ (B). Thermal ellipsoids are drawn at the 50% probability level. A single enantiomer is shown.

Table 3. Selected Bond Distances (Å) and Angles (deg) for N-Zr$_1$Cl$_2$

Bond Distances			
Zr(1)−N(1)	2.0363(19)	Zr(1)−C(1)	2.406(2)
Zr(1)−Cl(2)	2.3999(7)	Zr(1)−Cl(1)	2.3964(6)
Zr(1)−C(2)	2.462(2)	Zr(1)−C(9)	2.506(2)
Zr(1)−C(3)	2.582(2)	Zr(1)−C(4)	2.615(2)
Si(1)−N(1)	1.753(2)	Si(1)−C(20)	1.859(3)
Si(1)−C(21)	1.867(3)	Si(1)−C(1)	1.876(2)
C(3)−C(10)	1.488(3)	C(10)−C(11)	1.373(3)
Angles			
N(1)−Zr(1)−Cl(2)	112.25(6)	N(1)−Zr(1)−Cl(1)	104.41(6)
Cl(2)−Zr(1)−Cl(1)	104.53(2)	N(1)−Zr(1)−C(1)	72.19(8)
C(1)−Zr(1)−Si(1)	38.33(6)	N(1)−Si(1)−C(20)	114.18(11)
C(20)−Si(1)−C(21)	109.82(13)	Si(1)−N(1)−Zr(1)	105.65(9)
N(1)−Si(1)−C(1)	93.05(10)	C(11)−C(10)−C(3)	120.0(2)
C(19)−C(10)−C(3)	120.9(2)	N(1)−C(22)−C(23)	108.9(2)
C(14)−C(19)−C(10)	118.6(2)	C(4)−C(3)−C(10)	123.6(2)

1 is 359.6(5)°, indicating that atoms Si(1), N(1), C(12), and Zr(1) are essentially coplanar, which is also true for the atoms around dimethylamide atoms N(2) and N(3). Such coplanar structures suggest π bonding between the Zr and nitrogen atoms involving the nitrogen atom lone pair electrons.[9] The sum of bond angles around ring carbon atom C(1) is 352.0°, indicating the C(1)−Si(1) bond vector is displaced slightly from the ring plane due to the constrained geometry. As expected from previous structural results for analogous complexes,[3f] the carbon atoms of the Cp ring do not have equal bond distances to the Zr center. The Zr(1)−C(1) bond length (2.4725(18) Å) is the shortest while the Zr-(1)−C(4) bond length (2.6267(18) Å) is the longest.

II. Monometallic Complex {1-Me$_2$Si[3-(1)-naphthylindenyl](^{t}BuN)}ZrCl$_2$ (N-Zr$_1$Cl$_2$). A summary of crystal structure data for complex N-Zr$_1$Cl$_2$ is compiled in Table S2. Selected bond distances and angles for N-Zr$_1$Cl$_2$ are summarized in Table 3. As expected, the metrical parameters in Table 3 suggest that the Me$_2$Si bridge again forces the indenyl plane to tilt, rendering the structure more open sterically. The N(1)−Zr(1) centroid angle is 103.14(8)°, slightly larger than that in complex **1** (100.67(6)°) and that in the ethylindenyl analogue Zr$_1$Cl$_2$ (102.87(6)°),[3f] presumably reflecting the steric influence of the naphthyl group. The metrical parameters about the metal center are quite similar to those previously reported in the ethylindenyl-substituted analogue Zr$_1$Cl$_2$, except for the Cl−Zr−Cl

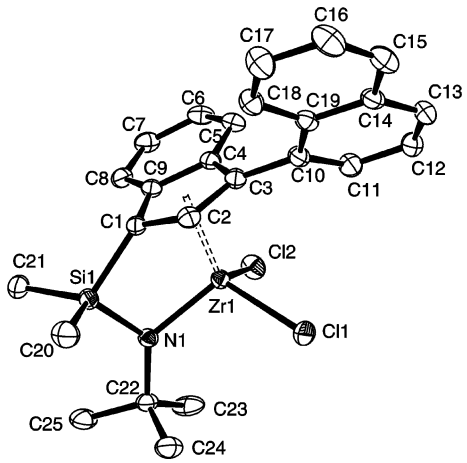

Figure 2. Molecular structure and atom numbering scheme for {1-Me$_2$Si[3-(1)-naphthylindenyl](^{t}BuN)}ZrCl$_2$ (N-ZrCl$_2$). Thermal ellipsoids are drawn at the 50% probability level. A single enantiomer is shown.

Table 4. Ethylene Polymerization Data for CGCZr Catalysts with Various Nuclearities and Cocatalysts[a]

entry no.	catalyst	μmol of cat.	reaction time (h)	polymer yield (g)	activity[b] (×10⁴)	ethyl branches per 1000C	*n*-butyl branches per 1000C	M_w[c] (×10²)	M_w/M_n[c]
1	$Zr_1 + B_2$[d]	10	1.16	1.08	9.3 (11)	6.5	0.6	6.9	1.1
2	C1-Zr_2 + B_2	5.0	1.50	0.19	1.3(3)	1.6	~0	880	2.7
3	C1-Zr_2 + B_1	5.0	1.50	0.29	1.9(3)	1.3	~0	495	2.3
4	C2-Zr_2 + B_2[d]	5.0	1.50	0.94	6.3 (7)	12	1.0	13	1.2
5	C2-Zr_2 + B_1[d]	5.0	1.25	1.09	8.7 (10)	2.7	~0	9.1	1.2
6	N-Zr_1 + B_2	10	1.50	0.51	3.4(7)	~0	~0	58	2.3
7	Zr_1Cl_2 + MAO[e]	10	1.50	0.37	2.5 (5)	~0	~0	12.4	1.2
8	C1-Zr_2Cl_4 + MAO[e]	5.0	1.50	0.38	2.5 (3)	~0	~0	6590	2.7
9	C2-Zr_2Cl_4 + MAO[e]	5.0	1.50	0.35	2.3 (5)	~0	~0	7500	2.8
10	N-Zr_1Cl_2 + MAO[e]	10	1.50	0.35	2.3 (5)	~0	~0	123	2.2
11	C1-Zr_2Cl_4 + MAO[f]	5.0	1.50	0.40	2.7 (3)	~0	~0	7390	2.6

[a] Polymerizations carried out on high vacuum line at 24 °C in 100 mL of toluene under 1.0 atm ethylene pressure. [b] In (g of polymer) (mol of cationic metallocene)$^{-1}$ atm^{-1} h^{-1}. [c] From GPC vs polystyrene standards. [d] From ref 3e (other low-M_w samples have a similarly low polydispersity pattern, likely reflecting imprecision in calibration). [e] Al:Zr = 1000:1. MAO dried in vacuo for 48 h to remove excess Al_2Me_6. [f] Al:Zr = 3000:1

Scheme 3. Ethyl Branch Formation Facilitated by Binuclear Macromonomer Binding

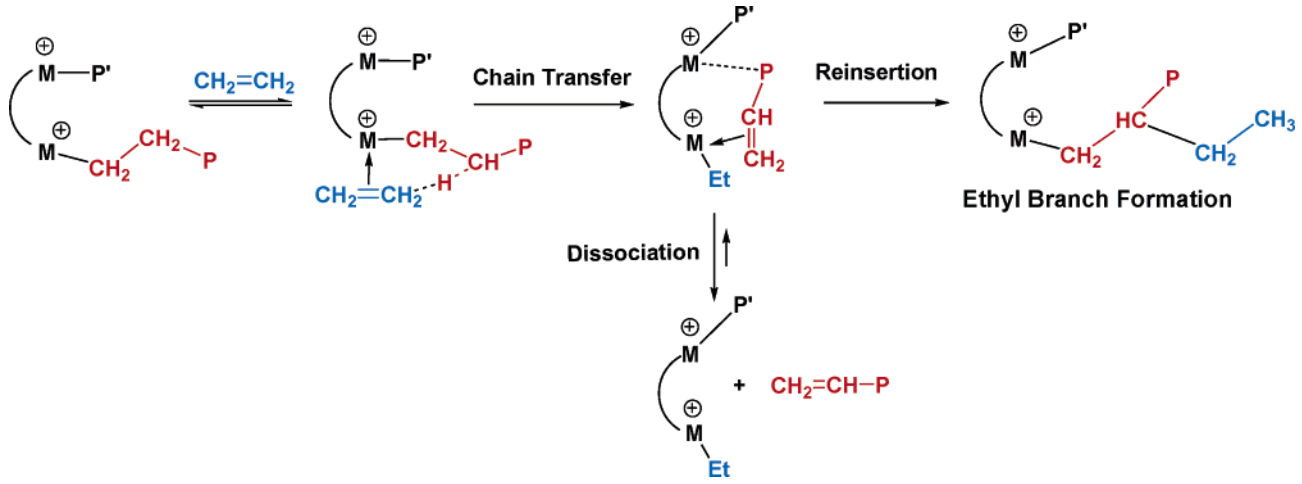

angle: the more hindered naphthylindenyl structure apparently induces the chlorine atoms to be slightly less widely spaced (angle Cl−Zr−Cl = 104.53(2)° vs 106.07(3)°).[3f] The dihedral angle between the indenyl and naphthyl ring is 121.5(2) °C. Similar to bimetallic complex **1**, the sum of the bond angles around bridge-connected nitrogen atom N(1) in N-Zr_1Cl_2 is close to 360 °C, indicating the atoms around N(1) are essentially coplanar and suggesting strong Zr−N bonding, again involving π-donation.[9] Because of the more electronegative character of the Cl ligands, the Zr center in N-Zr_1Cl_2 is expected to be more electron-deficient, and this leads to a shorter Zr−N(1) bond length and shorter Zr−C(ring) contacts in N-Zr_1Cl_2 than in **1**: Zr(1)−N(1) is 2.0363(19) Å in N-Zr_1Cl_2 vs 2.0980(16) Å in **1**; Zr(1)−C(1) is 2.406(2) Å in N-Zr_1Cl_2 vs 2.4725(18) Å in **1**.

Polymerization Studies. I. Catalytic Center Proximity Effects. Polymerizations were carried out using rigorously anhydrous/anaerobic methodology with attention to exotherm and mass transfer effects, as described previously.[3a,b] Additionally, in situ ^{1}H NMR spectroscopy verified rapid, quantitative Ph_3CCH_3 formation upon catalyst activation. The ethylene homopolymerization results are summarized in Table 4. The narrow monomodal polydispersities observed for the polyolefin products are consistent with well-defined single-site processes.[2] Entries 1, 2, and 4 reveal that 70× and 130× increases in M_w are achieved with C1-Zr_2 vs C2-Zr_2 and Zr_1, respectively, under identical polymerization conditions (B_2 as the cocatalyst). For single-site polymerizations, $M_{n,w}$ values are typically proportional to the net rate of chain propagation divided by the net rate of all chain termination processes (eq 1).[2]

$$M_n \propto \frac{R_{propagation}}{R_{termination}} \quad (1)$$

Presumably because of the greater steric hindrance exerted by the shorter bridge, the C1-Zr_2 polymerization activity is found to be ~20% that of C2-Zr_2 (Table 4, entries 2 and 4), and reasonably assuming comparable percentages of active catalytic centers,[10] this infers that the net rate of C1-Zr_2 propagation with borate cocatalysts is ~20% that of C2-Zr_2, hence, that the C1-Zr_2 termination kinetics must be substantially depressed in order to obtain the large observed M_w enhancement.

In terms of chain architecture, both C1-Zr_2 + B_2 and C2-Zr_2 + B_2 produce polyethylenes with ethyl branching as a distinctive microstructural feature. Moreover, the M_ws of the polyethylene products from the above catalyst systems are found to be essentially independent of ethylene pressure over a 0.5−5.0 atm range. Chain transfer to monomer[11,12] is therefore a probable source of ethyl branching in these systems, as suggested previously for C_2-Zr_2 + B_2[3f] (Scheme 3). As for branching levels, C2-Zr_2 + B_2 gives ~7.5× greater ethyl branches/1000 C than does C1-Zr_2 + B_2, meaning that the relative rate of ethyl generating chain transfers to normal propagation is ~7.5× greater for the former catalyst. As shown in Scheme 3, if ethyl branch formation arises predominately via chain transfer to monomer and subsequent intramolecular macromonomer reinsertion

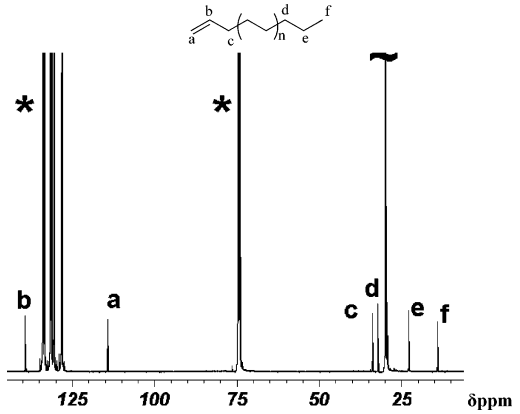

Figure 3. ^{13}C NMR spectrum (100 MHz, $C_2D_2Cl_4$, 120 °C) of the polyethylene produced by the catalyst Zr_1 + B_2 (Table 4, entry 1).

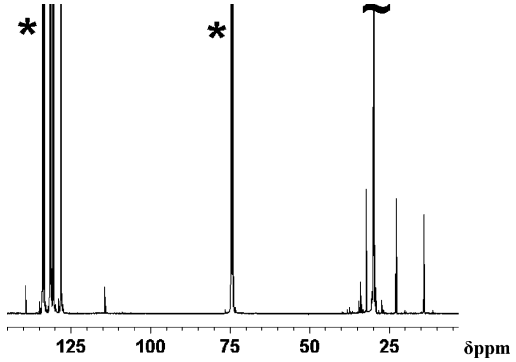

Figure 4. ^{13}C NMR spectrum (100 MHz, $C_2D_2Cl_4$, 120°) of the polyethylene produced by the catalyst Zr_1Cl_2 + MAO (Table 4, entry 7).

Scheme 4. Chain Transfer to Aluminum as a Termination Step

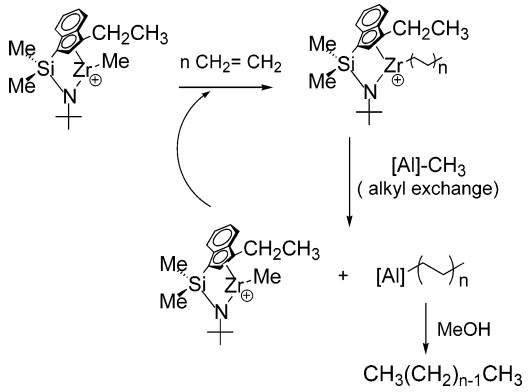

(at least for low degrees of conversion),[3f] then the average number of ethyl branches per polymer chain provides information on the relative rates of macromonomer reinsertion and dissociation in these two catalysts. The calculated average number of ethyl branches is 3.7 per polymer chain in the C1-Zr_2 + B_2-derived product, ~4× greater than that for C2-Zr_2 + B_2 (Table 4, entries 2 and 4), meaning that in C1-Zr_2 + B_2 the relative rate of macromonomer reinsertion to dissociation is ~4× greater than that in C2-Zr_2 + B_2. The closer achievable Zr−Zr distance in C1-Zr_2 + B_2 ion pair may increase the selectivity for macromonomer binding and thus enhance the probability of reinsertion (see additional discussion below).

II. Cocatalyst Effects. In regard to cocatalyst/ion pairing effects, with MAO as the cocatalyst, while the mononuclear Zr_1Cl_2 and N-Zr_1Cl_2 polymerization characteristics approximately parallel those of Zr_1 + B_2 and N-Zr_1 + B_2 (Table 4, entries 7, 10 vs entries 1, 6) in that all yield low M_w products, C1-Zr_2Cl_4 + MAO and C2-Zr_2Cl_4 + MAO both afford *very high and comparable* M_w polyethylenes, with M_w increased up to ~600× vs Zr_1Cl_2 (entries 8, 9 vs 7).[13] From Table 4, note that the C1-Zr_2Cl_4 + MAO and C2-Zr_2Cl_4 + MAO polymerization activities are similar to that of Zr_1Cl_2 + MAO, so using the arguments outlined above chain transfer rates must be substantially depressed in both binuclear catalysts. Comparing entries 8, 9, and 2, note that the MAO-activated species produce even higher molecular weight polyethylene than does C1-Zr_2 + B_2, with the lower ethyl branch content suggesting a scenario where the relative chain termination rate is even slower in Zr_2Cl_4 + MAO than in C1-Zr_2 + B_2 (ethyl branch formation requires chain transfer to monomer and subsequent α-olefin/polyolefin reinsertion, Scheme 3). Larger Al/Zr ratios do not change the polymerization behavior greatly, yielding slightly increased polymerization activity and polymer M_w (Table 4, entry11).

End-group analysis of the polyethylene products by ^{13}C NMR shows significant differences in the chain termination pathways in the presence of the different cocatalysts. With mononuclear Zr_1 as the catalyst and B_2 as the cocatalyst (Table 4, entry 1), the vinyl CH_2=CH−CH−:saturated $-CH_2CH_2CH_3$ end group ratio is 1:1 (as shown in Figure 3), consistent with a β-H transfer process as the predominant chain termination pathway. However, with MAO as the cocatalyst in this reaction (Table 4, entry 7), the vinyl CH_2=CH−CH−:−$CH_2CH_2CH_3$ end-group ratio is ~1:3 (Figure 4), arguing that a significant fraction of polymer chains have saturated $-CH_2CH_2CH_3$ moieties at both termini and that the ratio of vinyl-terminated chains:completely saturated chains is ~1:1 (the high molecular weight of the Zr_2Cl_4-derived polymer precludes end-group detection by ^{13}C NMR). Note that the MAO used here was dried in high vacuo for 48 h to remove excess Al_2Me_6. In MAO-cocatalyzed, H_2-free single-site catalysis, saturated chain ends are usually obtained via chain transfer to Al (Scheme 4).[14] While chain transfer to Al is typically considered a minor pathway in most MAO-activated single-site polymerization processes in the absence of additional aluminum alkyl,[14] and previous reports suggest sterically crowded ancillary ligand structures facilitate the chain transfer to Al,[15] the present observation shows that sterically open CGC structures can also render this chain transfer pathway accessible.[16]

For the in situ generated C1-Zr_2Cl_4 + MAO and C2-Zr_2Cl_4 + MAO catalysts, we observe a resonance in the ^1H NMR at δ −2.13 ppm, assignable to a Zr(μ-methyl)-Zr moiety (Figure 5A). Such a feature is not detectable in either the Zr_1Cl_2 + MAO, C1-Zr_2+ B_2, or C2-Zr_2+ B_2 reaction mixtures, but can also be detected in C2-Zr_2 + tris(perfluorobiphenyl)borane (PBB) reaction mixtures (1:1), where weakly coordinating H_3CPBB^- is known to readily stabilize Zr(μ-methyl)Zr moieties (Figure 5B).[17b] (In Figure 5B, because different diastereomers are all accessible, the other part of the spectrum is complicated and cannot be unambiguously assigned.) After introduction of ethylene to the C2-Zr_2Cl_4 + MAO reaction mixture, the relative intensity of the δ −2.13 peak decreases dramatically, consistent with μ-methyl scission and subsequent activation of the Zr centers, analogous to previous observations on other MAO-

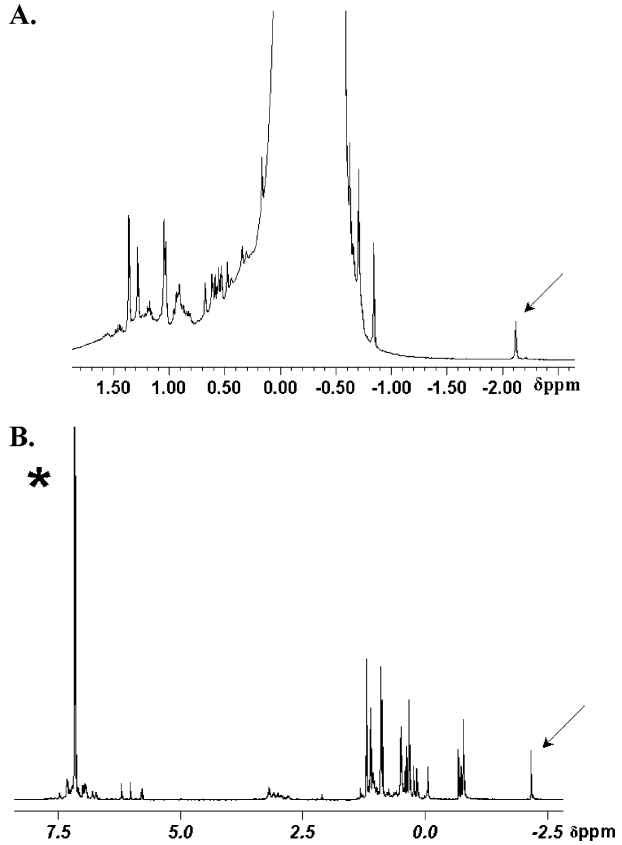

Figure 5. (A) ^{1}H NMR spectrum (400 MHz, C_6D_6, 23 °C) of the C1-Zr_2Cl_4 + MAO reaction mixture (Table 4, entry 8). (B) ^{1}H NMR spectrum (400 MHz, C_6D_6, 23 °C) of the C2-Zr_2 + PBB reaction mixture. The arrows identify resonances assignable by their characteristic field positions to M(μ-CH_3)M^+ species as discussed in the text.

activated metallocene μ-methyl species.[17a] This NMR information suggests that the two Zr centers can approach very closely[17] and that the bulky[18] MAO cocatalyst/counteranion can stabilize μ-methyl structures (e.g., **1**), similar to the stabilization of M(μ-CH_3)M^+ species by encumbered H_3CPBB^-.[17b] Taking the polymerization and NMR results on the MAO-derived ion pairs together, it is conceivable that MAO-enabled close proximity of the metal centers is an important factor in achieving high-M_w polyethylene products, similar to results in the borate-activated catalytic systems.

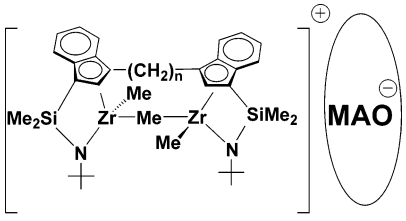

1

In regard to binuclear effects of cocatalyst B_2 vs mononuclear B_1, it can be seen that with C2-Zr_2 as the catalyst B_2 affords ~4.4× more ethyl branches and ~1.4× higher M_w than mononuclear B_1 (Table 4, entries 4 and 5). With C1-Zr_2 as the catalyst, B_2 yields ~1.2× more ethyl branches and ~1.7× higher M_w than B_1 (Table 4, entries 2 and 3). The higher branching and M_ws achieved by the binuclear cocatalyst is conceivably due to closer Zr···Zr proximity achieved by ion pairing with the binuclear counteranion (see discussion below).

III. Copolymerizations. Regarding metal−metal cooperative effects in olefin copolymerizations, note that the ethylene + 1-hexene experimental results are summarized in Table 5.[19] It can be seen that C1-Zr_2 + B_2 incorporates ~3× more 1-hexene than does C2-Zr_2 + B_2 under identical polymerization conditions (Table 5, entries 2 and 3). Interestingly, ^{13}C NMR data also reveal that the C1-Zr_2 + B_2-derived copolymer contains similar quantities of ethyl branches as in the above ethylene homopolymerizations, arguing that the same or a very similar chain transfer mechanism is again operative. Paralleling the homopolymerization results, the copolymer M_w is ~40× greater for the C1-Zr_2 + B_2-catalyzed copolymerization than for that mediated by C2-Zr_2 + B_2. With MAO as the copolymerization cocatalyst, C1-Zr_2Cl_4 incorporates 4.2× more, and C2-Zr_2Cl_4 3.5× more, 1-hexene than does Zr_1Cl_2 and with comparable polymerization activities for both catalyst systems (Table 5, entries 4−6). These comonomer enchainment selectivity data suggest that differences in achievable Zr···Zr proximities and structures likely facilitate comonomer enchainment (such as a π-olefin and agostic bound structure, **2**, the essential components of which find much precedent in d^0 olefin polymerization chemistry[20−22]). Paralleling the homopolymerizations, the copolymer M_w from the C1-Zr_2Cl_4- and C2-Zr_2Cl_4-mediated polymerizations is again significantly greater (~600×) than in the Zr_1Cl_2-catalyzed process (entries 4−6).

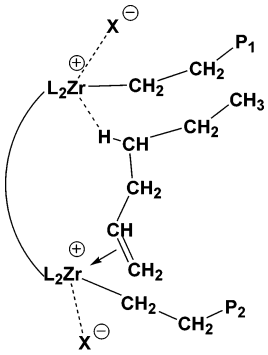

2

IV. Catalyst Steric and Polar Solvent Effects on Polymerization and Copolymerization. To better understand catalyst steric vs second metal proximity effects on the enchainment processes, the sterically encumbered mononuclear naphthyl derivative N-Zr_1 was also synthesized. Note that the polymerization and copolymerization results with N-Zr_1 (Table 4, compare entries 2, 6, and 10) argue that the effect of the proximate metal center on the polymerization processes is unlikely to be simply steric in origin. Furthermore, previous reports concerning mononuclear CGC catalyst structure effects on polyolefin molecular weight do not evidence clear steric trends when using borate as the cocatalyst.[23]

Polymerization results in more polar C_6H_5Cl (ϵ = 5.68, Table 6), which is expected to weaken ion pairing, evidence significant solvent effects. Compared with polymerizations conducted in toluene (ϵ = 2.38), more polar C_6H_5Cl dramatically increases polymerization activity, while there are negligible solubility differences

Table 5. Ethylene + 1-Hexene Copolymerization Data for CGCZr Catalysts with Various Nuclearities and Cocatalysts[a]

entry no.	catalyst	μmol of cat.	reaction time (h)	polymer yield (g)	activity[b] (×10⁴)	ethyl branches per 1000C	*n*-butyl branches per 1000 C	M_w[c] (×10²)	M_w/M_n[c]
1	$Zr_1 + B_2$[d]	10	0.75	1.00	13.3(13)	6.0	3.2	8.0	1.1
2	C1-$Zr_2 + B_2$	5.0	1.50	0.13	0.86(5)	1.3	17.2	508	2.3
3	C2-$Zr_2 + B_2$[d]	5.0	1.25	1.09	8.7 (9)	10	5.5	13	1.2
4	Zr_1Cl_2 + MAO[e]	10	1.50	0.46	1.5 (3)	~0	5.4	4.4	1.3
5	C1-Zr_2Cl_4 + MAO[e]	5.0	1.50	0.33	1.1 (2)	~0	22.8	3280	2.9
6	C2-Zr_2Cl_4 + MAO[e]	5.0	3.00	0.27	0.89 (6)	~0	19.4	2530	2.9

[a] Polymerizations carried out on a high-vacuum line at 24 °C in 100 mL of toluene under 1.0 atm ethylene pressure, [hexene] = 0.8 M. [b] In (g of polymer) (mol of cationic metallocene)$^{-1}$ atm^{-1} h^{-1}. [c] From GPC vs polystyrene standards. [d] From ref 3e (other low-M_w samples have a similarly low polydispersity pattern, likely reflecting imprecision in calibration). [e] Al:Zr = 1000:1. MAO dried in vacuo for 48 h to remove excess Al_2Me_6.

Table 6. Ethylene and Ethylene + 1-Hexene Polymerization Data Conducted in C_6H_5Cl[a]

entry no.	catalyst	monomer	μmol of cat.	reaction time (min)	polymer yield (g)	activity[b] (×10⁵)	ethyl branches per 1000C	*n*-butyl branches per 1000 C	M_w[c] (×10³)	M_w/M_n[c]
1	$Zr_1 + B_2$	E	10	1.5	0.17	6.8(3)	1.7	1.1	2.4	1.4
2	C2-$Zr_2 + B_2$	E	5.0	1.5	0.14	5.6 (2)	7.0	2.4	3.1	1.5
3	C1-Zr_2 +B_2	E	5.0	1.5	0.16	6.4(2)	2.8	1.4	2.4	1.6
4	C1-Zr_2Cl_4 + MAO[d]	E	5.0	15	0.35	1.4(2)	~0	~0	380	2.5
5	$Zr_1 + B_2$	E/H	10	2.0	0.28	8.4(5)	1.7	35.1	3.8	1.4
6	C2-Zr_2 +B_2	E/H	5.0	2.0	0.26	7.8(5)	5.6	44.9	2.5	1.5
7	C1-$Zr_2 + B_2$	E/H	5.0	2.0	0.19	5.7 (7)	2.2	48.3	3.8	1.8

[a] Polymerizations carried out on a high-vacuum line at 24 °C in 100 mL of C_6H_5Cl under 1.0 atm ethylene pressure, [hexene] = 0.8 M. [b] In (g of polymer) (mol cationic metallocene)$^{-1}$ atm^{-1} h^{-1}. [c] From GPC vs polystyrene standards. [d] Al:Zr = 1000:1. MAO dried in vacuo for 48 h to remove excess Al_2Me_6.

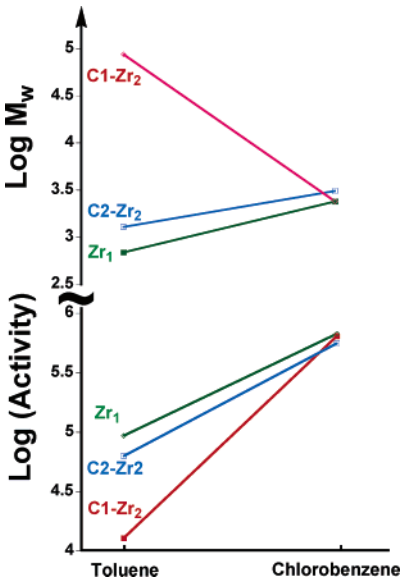

Figure 6. Log(polymerization activity) and log(polymer M_w) in ethylene homopolymerization in toluene or chlorobenzene (B_2 as cocatalyst, Table 4, entries 1, 2, 4 vs Table 6, entries 1, 2, 3).

for ethylene in toluene and in chlorobenzene.[24] In ethylene homopolymerization, activities are enhanced ~50× for C1-Zr_2 + B_2, ~9× for C2-Zr_2 + B_2, and ~7× for Zr_1+ B_2 in C_6H_5Cl vs those conducted in toluene (compare Table 6, entries 1, 2, 3 with Table 4, entries 1, 2, 4,). In toluene, the polymerization activity decreases as catalyst steric hindrance increases (sterically most encumbered C1-Zr_2 + B_2 exhibits an activity only ~20% of that of C2-Zr_2 + B_2 and 14% of that of Zr_1 + B_2), while in polar C_6H_5Cl, the activities of the above three catalysts are comparable, as shown in Figure 6. Such a compression in activity dispersion agrees with previous results,[25,26] arguing that in polar solvents catalyst−cocatalyst ion pairing is significantly weakened and that sterically hindered structures which exhibit low polymerization activity in toluene become "freer" cations, exhibiting activities comparable to those of their less-crowded analogues. Similar compression in catalytic activity dispersion in polar solvents was found in propylene polymerizations mediated by ion pairs having significantly different degrees of "tightness" in nonpolar solvents.[25a]

Significantly, the M_ws of polymers produced by C1-Zr_2 + B_2 fall precipitously in chlorobenzene compared with those produced in toluene. In ethylene homopolymerization, the M_w of polymer produced by C1-Zr_2 + B_2 falls to 2400, only ~3% of that produced in toluene, while the M_w of the polymers produced by C2-Zr_2 + B_2 and Zr_1 + B_2 are 3100 and 1200, respectively—perhaps slightly increased from those produced in toluene. The M_ws of the polymers derived from all three catalysts (C1-Zr_2 + B_2, C2-Zr_2 + B_2, and Zr_1+ B_2) are in the same range. As shown in Figure 6, the dramatic M_w enhancement effects for C1-Zr_2 + B_2 vs C2-Zr_2 + B_2, which are observed in toluene, are substantially suppressed in more polar C_6H_5Cl. In ethylene + 1-hexene copolymerization, similar trends in M_w compression are observed: the M_ws of the copolymers are 3800 for C1-Zr_2 + B_2, ~2500 for C2-Zr_2 + B_2, and ~3800 for Zr_1+ B_2 in C_6H_5Cl (Table 6, entries 5−7).

In terms of cocatalyst sensitivity in the C_6H_5Cl experiments, MAO is found to behave quite differently from the borate cocatalysts: for C1-Zr_2Cl_4 + MAO, the activity enhancement in C_6H_5Cl vs toluene is ~4×, not as great as found in borate-activated systems. More importantly, the product M_w declines only slightly compared with that in toluene (Table 6, entry 4 vs Table 4, entry 8). These data suggest, not surprisingly, that as a cocatalyst MAO has a significantly different single-site catalyst activation behavior and ion-pairing interactions than do borate cocatalysts, especially in the case of binuclear Zr complexes (see discussion below).

In ethylene homopolymerization carried out in C_6H_5-Cl, ethyl branching is still the predominant type of branch microstructure formed, with branching at the same level or lower in the polymers produced in C_6H_5-

Cl vs those in toluene. For C2-Zr_2 + B_2, 7.0 ethyl branches/1000 C are achieved in C_6H_5Cl vs 12 ethyl branches/1000 C in toluene; for C1-Zr_2 + B_2, 1.7 ethyl branches/1000 C are produced in C_6H_5Cl vs 1.6 ethyl branches/1000 C in toluene. In ethylene + 1-hexene copolymerization, the comonomer incorporation levels for both mononuclear and binuclear catalysts increase significantly in C_6H_5Cl vs those in toluene. The enhancement is ~11× in Zr_1 + B_2, ~8× in C2-Zr_2 + B_2, and ~3× in C1-Zr_2 + B_2 (Table 6, entries 5−7). In previous reports of single-site propylene/1-hexene copolymerizations,[25b,e] significantly greater 1-hexene incorporation levels are also observed in more polar C_6H_5Cl vs those in toluene. These results suggest that "freer" cationic species generated in polar solvents are more accessible to the relatively bulky comonomers. Taken together, these results indicate that the strength of the catalyst−cocatalyst ion pairing, as modulated by the polarity of the polymerization medium, plays a significant role in a number of aspects of the multinuclear enchainment process (see Discussion below).

Discussion

I. Bimetallic Proximity Effects. From the results outlined above, the significantly enhanced polymer product molecular weight in C1-Zr_2- vs C2-Zr_2-mediated polymerizations, and the relative activities of the two catalysts, suggests that the termination rates must be substantially depressed for C1-Zr_2. These effects plausibly reflect access to bridged structures in which proximate metal centers may coordinate/stabilize the growing polymer chain, possibly via agostic interactions as suggested in structure **3** for which there is mono-

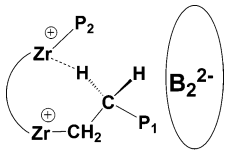

3

nuclear precedent,[20] thereby impeding chain transfer to monomer and subsequent macromonomer dissociation as a chain termination pathway and thus significantly reducing the overall chain termination rate. Green et al. proposed the possibility of a similar effect[3h,j] in bimetallic metallocene catalyst systems as a route to high-M_w polyolefins; however, probably as a consequence of the sterically/coordinatively encumbered nature of the catalysts investigated, substantial cooperative effects were minimal. The present ethylene/1-hexene copolymerization results also reveal that shorter bridged catalyst C1-Zr_2 incorporates more comonomer than C2-Zr_2 under identical reaction conditions, presumably reflecting more favorable metal−comonomer binding, leading to greater cooperative effects.

The significant energetic differences in the conformation of the C1- and C2-bridged catalyst structures (Figure 1A vs Figure 1B) also suggest that cooperative effects may be more accessible in C1-Zr_2 than in C2-Zr_2. Molecular modeling[27] results based on the crystal structures show that the more constricted geometry in methylene-bridged binuclear MBICGC[$Zr(NMe_2)_2$]$_2$ incurs ~5 kcal/mol destabilization when the C2−C3−C21−C24 dihedral angle is increased 30° from crystallographically determined conformation and incurs ~63 kcal/mol destabilization for a 100° increase, as shown in **4**. In sharp contrast, in ethylene-bridged EBICGC-[$Zr(NMe_2)_2$]$_2$, the destabilization is ≤4 kcal/mol when the C9−C20−C20′−C9′ dihedral angle is rotated up to 180°.[27] The greater rigidity in the $-CH_2-$ bridged structure can enforce a close Zr···Zr proximity and thus favor conformations for metal−alkyl chain interactions (e.g., **3**).

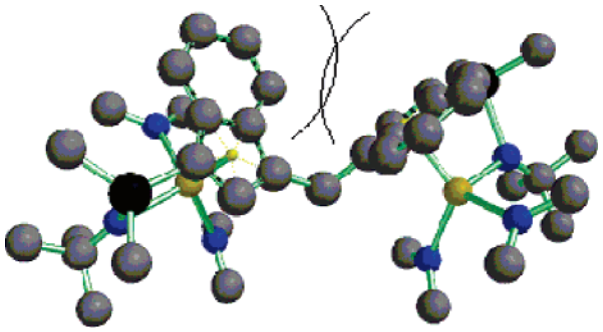

4

II. Cocatalyst Effects. The differences in ^{13}C NMR spectra of the polymeric products as a function of cocatalyst (Figures 3 and 4) indicate that the chain termination pathway is significantly different for MAO and borate cocatalysts. Not surprisingly, chain transfer to aluminum is a significant chain transfer pathway in the former case but is absent in the latter. The sharply different response to solvent polarity changes between the MAO- and borate-cocatalyzed processes also suggests that the ion-pairing properties and catalyst−cocatalyst interactions are significantly different in these two systems (see the solvent polarity discussion below).

The detection of Zr−(μ-CH_3)−Zr species in the ^1H NMR of the of the C1-Zr_2Cl_4 + MAO reaction product suggests that the two metal centers can attain close proximity in bimetallic catalysts when MAO is used as cocatalyst (e.g., **1**, Zr−(μ-CH_3)−Zr distances are typically ~4.8−4.9 Å[17b,28]). Admittedly, the Zr−μ-Me−Zr linkage undergoes scission during the polymerization process; however, the Zr···Zr units may still attain close average proximity. In fact, with MAO as the cocatalyst, the methylene and $-CH_2CH_2-$ bridged catalysts exhibit comparable catalytic response, arguing that the bulky MAO counteranion may force the two metal centers into proximity such that differences in bridge length are no longer a crucial factor. These results suggest that, as a cocatalyst, MAO can significantly influence the metal−metal proximity in the binuclear catalyst systems, thus modulating chain termination pathways.

In terms of binuclear effects observed with dianionic cocatalysts, the greater branching and M_w achieved by binuclear cocatalyst B_2 vs mononuclear B_1 can be tentatively explained by closer accessible Zr···Zr proximity and electrostatically optimized ion pair spatial conformations which would hold the propagating chains in closer proximity (e.g., **5**) vs that with two monoanions (e.g., **6**). It is conceivable that *bulky* MAO can also generate ion pairs with conformations similar to **5**, thus accessible to binuclear cooperative effects.

III. Solvent Polarity Effects. The polymerization results with more polar C_6H_5Cl reveal that polymer M_w and comonomer enchainment are highly dependent on the catalyst−cocatalyst ion pairing. Previous studies have shown that polar solvents can weaken the cation−anion interaction, enhance the ion-pair mobility,[26] and render the cation "freer" with greater polymerization

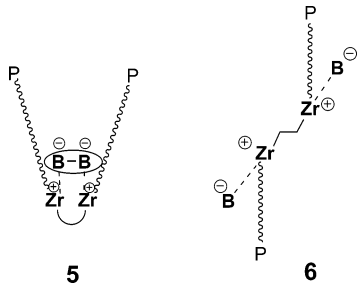

5 **6**

activity.[25] The present results reveal similar trends in terms of solvent effects on polymerization activity. Notably, with C_6H_5Cl as the solvent for C1-Zr_2 + B_2, C2-Zr_2 + B_2, and Zr_1+ B_2, having varied nuclearity and steric characteristics, a dramatic compression in the polymerization activity and molecular weight dispersion is found vs toluene as the solvent, as shown in Figure 6. We previously reported similar observations in syndiospecific propylene polymerization mediated by C_s-symmetric metallocenium catalysts[25a]—dramatic compression in the dispersion of polymerization rates and tacticity in polar 1,3-dichlorobenzene vs in toluene.

It has also been reported that polar solvents can compete for/coordinate with electrophilic metal centers and can weaken/supplant agostic interactions.[29] In single-site polymerizations, solvent polarity can play an important role in the transition states for chain termination processes involving metal center−β-H agostic interactions.[29b] The proposed effects in structure **2** and/or **3** for M_w enhancement and comonomer selectivity in C1-Zr_2 would thus be suppressed in more polar solvents, e.g., **3**, **7** for which there is extensive mononuclear precedent.[20,25,29]

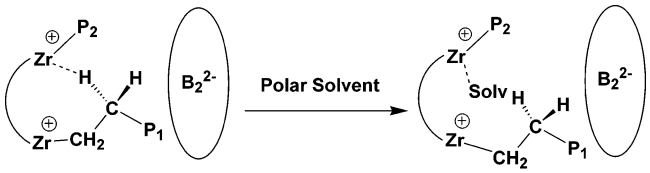

3 **7**

Summary

The present results significantly expand the scope of what is known about metal−metal proximity and cocatalyst/solvent effects in binuclear CGC olefin polymerization catalysis. In ethylene homopolymerization, ~70× increases in molecular weight are achieved with C1-Zr_2 vs C2-Zr_2 under identical polymerization conditions with B_2 as the cocatalyst in toluene. With MAO as the cocatalyst, ~600× increases in polyethylene molecular weight are achieved with C2-Zr_2Cl_4 and C1-Zr_2Cl_4 vs mononuclear Zr_1Cl_2. In the ethylene + 1-hexene copolymerization, C1-Zr_2 enchains 3× more 1-hexene than C2-Zr_2 does under identical polymerization conditions (B_2 as cocatalyst). With MAO as the cocatalyst, C2-Zr_2Cl_4 enchains 3.5× more, and C1-Zr_2Cl_4 4.2× more, 1-hexene than Zr_1Cl_2 does. When polar C_6H_5Cl is used as the polymerization medium, thereby weakening the catalyst−cocatalyst ion pairing, substantial alterations in catalyst response and polymer product properties are observed. Both homopolymerization and copolymerization results argue that achievable Zr···Zr spatial proximity, as modulated by the ion pairing, significantly influences chain transfer rates and selectivity for comonomer enchainment and that such proximity effects are highly cocatalyst and solvent sensitive.

Acknowledgment. This research was supported by grants from NSF (CHE-0415407) and DOE (86ER13511). H.L. thanks Dr. L. Li, Dr. J. Wang, Dr. C. Zuccaccia, and Mr. N. Guo for helpful discussions.

Supporting Information Available: Details of crystal structures and CIF files. This material is available free of charge via the Internet at http://pubs.acs.org.

References and Notes

(1) (a) Sammis, G. M.; Danjo, H.; Jacobsen, E. N. *J. Am. Chem. Soc.* **2004**, *126*, 9928−9929. (b) Iranzo, O.; Kovalevsky, A. Y.; Morrow, J. R.; Richard, J. P. *J. Am. Chem. Soc.* **2003**, *125*, 1988−1993. (c) Trost, B. M.; Mino, T. *J. Am. Chem. Soc.* **2003**, *125*, 2410−2411. (d) Jacobsen, E. N. *Acc. Chem. Res.* **2000**, *33*, 421−431. (e) Molenveld, P.; Engbersen, J. F. J.; Reinhoudt, D. N. *Chem. Soc. Rev.* **2000**, *29*, 75−86. (f) Konsler, R. G.; Karl, J.; Jacobsen, E. N. *J. Am. Chem. Soc.* **1998**, *120*, 10780−10781. (g) Molenveld, P.; Kapsabelis, S.; Engbersen, J. F. J.; Reinhoudt, D. N. *J. Am. Chem. Soc.* **1997**, *119*, 2948−2949. (h) Mathews, R. C.; Howell, D. H.; Peng, W.-J.; Train, S. G.; Treleaven, W. D.; Stanley, G. G. *Angew. Chem., Int. Ed. Engl.* **1996**, *35*, 2253−2256. (i) Sawamura, M.; Sudoh, M.; Ito, Y. *J. Am. Chem. Soc.* **1996**, *118*, 3309−3310.

(2) For recent reviews of single site olefin polymerization, see: (a) Bochmann, M. *J. Organomet. Chem.* **2004**, *689*, 3982−3998. (b) Gibson, V. C.; Spitzmesser, S. K. *Chem. Rev.* **2003**, *103*, 283−316. (c) Pedeutour, J.-N.; Radhakrishnan, K.; Cramail, H.; Deffieux, A. *Macromol. Rapid Commun.* **2001**, *22*, 1095−1123. (d) Gladysz, J. A., Ed.; *Chem. Rev.* **2000**, *100* (special issue on "Frontiers in Metal-Catalyzed Polymerization"). (e) Marks, T. J.; Stevens, J. C., Eds.; *Top. Catal.* **1999**, *15*, and references therein. (f) Britovsek, G. J. P.; Gibson, V. C.; Wass, D. F. *Angew. Chem., Int. Ed.* **1999**, *38*, 428−447. (g) Kaminsky, W.; Arndt, M. *Adv. Polym. Sci.* **1997**, *127*, 144−187. (h) Bochmann, M. *J. Chem. Soc., Dalton Trans.* **1996**, 255−270. (i) Brintzinger, H.-H.; Fischer, D.; Mulhaupt, R.; Rieger, B.; Waymouth, R. M. *Angew. Chem., Int. Ed. Engl.* **1995**, *34*, 1143−1170. (j) *Catalyst Design for Tailor-Made Polyolefins*; Soga, K., Terano, M., Eds.; Elsevier: Tokyo, 1994. (k) Marks, T. J. *Acc. Chem. Res.* **1992**, *25*, 57−65.

(3) For studies of binuclear metallocenes, see: (a) Li, H.; Li, L.; Marks, T. J. *Angew. Chem., Int. Ed.* **2004**, *37*, 4937−4940. (b)Wang, J.; Li, H.; Guo. N.; Li, L.; Stern, C. L.; Marks, T. J. *Organometallics* **2004**, *23,* 5112−5114. (c) Guo, N.; Li, L.; Marks, T. J. *J. Am. Chem. Soc.* **2004**, *126*, 6542−43. (d) Li, H.; Li, L.; Marks, T. J. Liable-Sands, L.; Rheingold, A. L. *J. Am. Chem. Soc.* **2003**, *124*, 10788−10789. (e) Noh, S. K.; Lee, J.; Lee, D. *J. Organomet. Chem.* **2003**, *667*, 53−60. (f) Li, L.; Metz, M. V.; Li, H.; Chen, M.-C.; Marks, T. J.; Liable-Sands, L.; Rheingold, A. L. *J. Am. Chem. Soc.* **2002**, *124*, 12725−12741. (g) Abramo, G. P.; Li, L.; Marks, T. J. *J. Am. Chem. Soc.* **2002**, *124*, 13966−13967. (h) Green, M. L. H.; Popham, N. H. *J. Chem. Soc., Dalton Trans.* **1999**, 1049−1059 and references therein. (i) Spaleck, W.; Kuber, F.; Bachmann, B.; Fritze, C.; Winter, A. *J. Mol. Catal. A: Chem.* **1998**, *128*, 279−287. (j) Yan, X.; Chernega, A.; Green, M. L. H.; Sanders, J.; Souter, J.; Ushioda, T. *J. Mol. Catal. A: Chem.* **1998**, *128*, 119−141. (k) Soga, K.; Ban, H. T.; Uozumi, T. *J. Mol. Catal. A: Chem.* **1998**, *128*, 273−278. (l) Bochmann, M.; Cuenca, T.; Hardy, D. T. *J. Organomet. Chem.* **1994**, *484*, C10−C12.

(4) (a) Arndt, S.; Okuda, J. *Chem. Rev.* **2002**, *102*, 1953−1976. (b) Chum, P. S.; Kruper, W. J.; Guest, M. J. *Adv. Mater.* **2000**, *12*, 1759−1767. (c) McKnight, A. L.; Waymouth, R. M. *Chem. Rev.* **1998**, *98*, 2587−2598. (d) Harrison, D.; Coulter, I. M.; Wang, S. T.; Nistala, S.; Kuntz, B. A.; Pigeon, M.; Tian, J.; Collins, S. *J. Mol. Catal. A: Chem.* **1998**, *128*, 65−77. (e) Soga, K.; Uozumi, T.; Nakamura, S.; Toneri, T.; Teranishi, T.; Sano, T.; Arai, T.; Shiono, T. *Macromol. Chem. Phys.* **1996**, *197*, 4237−4251. (f) Devore, D. D.; Timmers, F. J.; Hasha, D. L.; Rosen, R. K.; Marks, T. J.; Deck, P. A.; Stern, C. L. *Organometallics* **1995**, *14*, 3132−3134. (g) Stevens, J. C. *Proc. MetCon Houston* **1993**, 157. (h) Lai, S. Y.; Wilson, J. R.; Knight, G. W.; Stevens, J. C. WO-93/08221, 1993. (i) Canich, J. M.; Hlatky, G. G.; Turner, H. W. PCT Appl. WO 92-00333, 1992. Canich, J. M. Eur. Patent Appl. EP 420 436-A1, 1991

(Exxon Chemical Co.) (j) Devore, D. D. European Patent Application EP-514-828-A1, Nov 25, 1992.
(5) Liu, W.; Ray, D. G. III; Rinaldi, P. L. *Macromolecules* **1999**, *32*, 3817−3819.
(6) Protivova, J.; Pospisil, J.; Zikmund, L. *J. Polym. Sci*., *Polym. Symp.* **1973**, *40* 233−243.
(7) Dang, V.; Yu, L.; Balboni, D.; Dall'Occo, T.; Resconi, L.; Mercandelli, P.; Moret, M.; Sironi, A. *Organometallics* **1999**, *18*, 3781−3791.
(8) Grimmer, N. E.; Coville, N. J.; Koning, C. B.; Smith, J. M.; Cook, L. M. *J. Organomet. Chem.* **2000**, *616*, 112−127.
(9) (a) Andersen, R. A.; Beach, D. B.; Jolly, W. L. *Inorg. Chem.* **1985**, *24*, 2741. (b) Lappert, M. F.; Power, P. P.; Sanger, A. R.; Srivastava, R. C. *Metal and Metalloid Amides*; Ellis Horwood: Chichester, West Sussex, U.K., 1980; pp 500−502. (c) Bradley, D. C.; Chisholm, M. H. *Acc. Chem. Res.* **1976**, *9*, 273−280.
(10) (a) Liu, Z.; Somsook, E.; Landis, C. R. *J. Am. Chem. Soc.* **2001**, *123*, 2915−2916. (b) Liu, Z.; Somsook, E.; White, C. B.; Landis, C. R. *J. Am. Chem. Soc.* **2001**, *123*, 11193−11207.
(11) (a) Izzo, L.; Riccardis, F. D.; Alfano, C.; Caporaso, L.; Oliva, L. *Macromolecules* **2001**, *34*, 2−4. (b) Wang, L.; Yuan, Y.; Feng, L.; Wang, Y.; Pan, J.; Ge, C.; Ji, B. *Eur. Polym. J.* **2000**, *36*, 851−855. (c) Izzo, L.; Caporaso, L.; Senatore, G.; Oliva, L. *Macromolecules* **1999**, *32*, 6913−6916.
(12) For theoretical studies of single-site chain transfer pathways, see: (a) Klesing, A.; Bettonville, S. *Phys. Chem. Chem. Phys.* **1999**, *1*, 2373−2377. (b) Froese, R. D. J.; Musaev, D. G.; Morokuma, K. *Organometallics* **1999**, *18*, 373−379. (c) Thorshaug, K.; Stovneng, J. A.; Rytter, E.; Ystenes, M. *Macromolecules* **1998**, *31*, 7149−7165. (d) Margl, P. M.; Woo, T. K.; Ziegler, T. *Organometallics* **1998**, *17*, 4997−5002.
(13) C1-Zr_2 + MAO exhibits polymerization behavior indistinguishable from that of C1-Zr_2Cl_4 + MAO, excluding artifacts due to Zr−Cl linkages.
(14) (a) Nabhriain, N.; Brintzinger, H.-H.; Ruchatz, D.; Fink, G. *Macromolecules* **2005**, *38*, 2056−2063. (b) Makio, H.; Koo, K.; Marks, T. J. *Macromolecules* **2001**, *34*, 4676−4679. (c) Byun, D. J.; Shin, D. K.; Kim, S. Y. *Polym. Bull. (Berlin)* **1999**, *42*, 301. (d) Leino, R.; Luttikhedde, H. J. G.; Lehmus, P.; Willen, C.; Sjoholm, R.; Lehtonen, A.; Seppala, J.; Nasman, J. H. *Macromolecules* **1997**, *30*, 3477−3483. (e) Rieger, B.; Reinmuth, A.; Roll, W.; Brintzinger, H. H. *J. Mol. Catal.* **1993**, *82*, 67. (f) Resconi, L.; Piemontesi, F.; Franciscono, G.; Abis, L.; Fiorani, T. *J. Am. Chem. Soc.* **1992**, *114*, 1025−1032. (g) Mogstad, A. L.; Waymouth, R. M. *Macromolecules* **1992**, *25*, 2282−2284.
(15) (a) Han, C. J.; Lee, M. S.; Byun, D.-J.; Kim, S. Y. *Macromolecules* **2002**, *35*, 8923−8925. (b) Götz, C.; Rau, A.; Luft, G. *Macromol. Mater. Eng.* **2002**, *287*, 16−22. (c) Lieber, S.; Brintzinger, H.-H. *Macromolecules* **2000**, *33*, 9192−9199.
(16) (a) In related single-site work with aluminum alkyls as chain transfer reagents in ethylene polymerization, CGC catalysts were found to be the more efficient than metallocene catalysts: Tian, S.; Marks, T. J., unpublished observations. For studies of analogous silane chain transfer, see: (b) Koo, K.; Fu, P.-F.; Marks, T. J. *Macromolecules* **1999**, *32*, 981−988. (c) Koo, K.; Marks, T. J. *J. Am. Chem. Soc.* **1998**, *120*, 4019−4020.
(17) (a) Tritto, I.; Donetti, R.; Sacchi, M. C.; Locatelli, P.; Zannoni, G. *Macromolecules* **1999**, *32*, 264−269. (b) Chen, Y.-X.; Metz, M. V.; Li, L.; Stern, C. L.; Marks, T. J. *J. Am. Chem. Soc.* **1998**, *120*, 6287−6305. (c) Beck, S.; Prosenc, M.-H.; Brintzinger, H.-H.; Goretzki, R.; Herfert, N.; Fink, G. *J. Mol. Catal.* **1996**, *111*, 67−79.
(18) Babushkin, D. E.; Brintzinger, H.-H. *J. Am. Chem. Soc.* **2002**, *124*, 12869−12873.
(19) We assume most *n*-butyl branches in the ethylene + 1-hexene copolymer are from 1-hexene incorporation since negligible *n*-butyl branching is detected in the ethylene homopolymer under these polymerization conditions (Table 4).
(20) (a) Scherer, W.; McGrady, G. S. *Angew. Chem., Int. Ed.* **2004**, *43*, 1782−1806. (b) Prosenc, M. H.; Brintzinger, H. H. *Organometallics* **1997**, *16*, 3889−3894. (c) Grubbs, R. H.; Coates, G. W. *Acc. Chem. Res.* **1996**, *29*, 85−93. (d) Prosenc, M. H.; Janiak, C.; Brintzinger, H. H. *Organometallics* **1992**, *11*, 4036−4041. (e) Cotter, W. D.; Bercaw, J. E. *J. Organomet. Chem.* **1991**, *417*, C1−C6. (f) Krauledat, H.; Brintzinger, H. H. *Angew. Chem., Int. Ed. Engl.* **1990**, *29*, 1412−1413. (g) Piers, W. E.; Bercaw, J. E. *J. Am. Chem. Soc.* **1990**, *112*, 9406−9407. (h) Brookhart, M.; Green, M. L. H.; Wong, L. L. *Prog. Inorg. Chem.* **1988**, *36*, 1−124. (i) Clawson, L.; Soto, J.; Buchwald, S. L.; Steigerwald, M. L.; Grubbs, R. H. *J. Am. Chem. Soc.* **1985**, *107*, 3377−3378.
(21) (a) Casey, C. P.; Tunge, J. A.; Lee, T.-Y.; Fagan, M. A. *J. Am. Chem. Soc.* **2003**, *125*, 2641−2651. (b) Landis, C. R.; Rosaaen, K. A.; Uddin, J. *J. Am. Chem. Soc.* **2002**, *124*, 12062−12063. (c) Casey, C. P.; Lee, T.-Y.; Tunge, J. A.; Carpenetti, D. W., II *J. Am. Chem. Soc.* **2001**, *123*, 10762−10763. (d) Grubbs, R. H.; Coates, G. W. *Acc. Chem. Res.* **1996**, *29*, 85−93.
(22) (a) Stoebenau, E. J., III.; Jordan, R. F. *J. Am. Chem. Soc.* **2004**, *126*, 11170−11171. (b) Stoebenau, E. J., III.; Jordan, R. F. *J. Am. Chem. Soc.* **2003**, *125*, 3222−3223. (c) Carpentier, J.-F.; Maryin, V. P.; Luci, J.; Jordan, R. F. *J. Am. Chem. Soc.* **2001**, *123*, 898−909.
(23) (a) Resconi, L.; Camurati, I.; Grandini, C.; Rinaldi, M.; Mascellani, N.; Traverso, O. *J. Organomet. Chem.* **2002**, *664*, 5−26.
(24) The solubility of ethylene is reported to be 0.117 mol/L in toluene[24a] and 0.118 mol/L in chlorobenzene[24b] at current polymerization conditions (25 °C, 1 atm): (a) Atiqullah, M.; Hammawa, H.; Hamid, H. *Eur. Polym. J.* **1998**, *34*, 1511−1520. (b) Sahgal, A.; La, H. M.; Hayduk, W. *Can. J. Chem. Eng.* **1978**, *56*, 354−357.
(25) (a) Chen, M.-C.; Roberts, J. A. S.; Marks, T. J. *J. Am. Chem. Soc.* **2004**, *126*, 4605−4625. (b) Forlini, F.; Tritto, I.; Locatelli, P.; Sacchi, M. C.; Piemontesi, F. *Makromol. Chem. Phys.* **2000**, *201*, 401−408. (c) Kleinschmidt, R.; Griebenow, Y.; Fink, G. *J. Mol. Catal. A: Chem.* **2000**, *157*, 83−90. (d) Coevoet, D.; Cramail, H.; Deffieux, A. *Makromol. Chem. Phys.* **1999**, *200*, 1208−1214. (e) F. Forlini, F.; Fan, Z. Q.; Tritto, I.; Locatelli, P.; Sacchi, M. C. *Macromol. Chem. Phys.* **1997**, *198*, 2397−2408. (f) Herfert, N.; Fink, G. *Makromol. Chem.* **1992**, *193*, 773−778.
(26) (b) Beswick, C. L.; Marks, T. J. *J. Am. Chem. Soc.* **2000**, *122*, 10358−10370. (b) Deck, P. A.; Beswick, C. L.; Marks, T. J. *J. Am. Chem. Soc.* **1998**, *120*, 1772−1784.
(27) These calculations began with the crystallographic conformations of **1** and EBICGC[$Zr(NMe_2)_2$]$_2$ using the following procedure. First, the mol2 files of the original crystal structures were loaded into the Spartan 2002 Windows program (Wavefunction, Inc., Irvine, 2001). Next, the dihedral angle around the bridge was rotated to varying degrees and the single point energy of the structure calculated at the MP3 level.
(28) (a) Chen, M.; Roberts, J. A. S.; Seyam, A. M.; Li, L.; Zuccaccia, C.; Stahl, N. G.; Marks, T. J. Manuscript in preparation. (b) Duncan, A. P.; Mullins, S. M.; Arnold, J.; Bergman, R. G. *Organometallics* **2001**, *20*, 1808−1819. (c) Schrock, R. R.; Casado, A. L.; Goodman, J. T.; Liang, L.-C.; Bonitatebus, Jr. P. J.; Davis, W. M. *Organometallics* **2000**, *19*, 5325−5341.
(29) (a) Bouwkamp, M. W.; de Wolf, J.; del Hierro Morales, I.; Gercama, J.; Meetsma, A.; Troyanov, S. I.; Hessen, B.; Teuben, J. H. *J. Am. Chem. Soc.* **2002**, *124*, 12956−12957. (b) Kawabe, M.; Murata, M. *Macromol. Chem. Phys.* **2001**, *202*, 2440−2446. (c) Rybtchinski, B.; Konstantinovsky, L.; Shimon, L. J. W.; Vigalok, A.; Milstein, D. *Chem.—Eur. J.* **2000**, *6*, 3287−3292. (c) Carr, N.; Mole, L.; Orpena, A. G.; Spencer, G. L. *J. Chem. Soc., Dalton Trans.* **1992**, *18*, 2653−2662. (d) Agbossou, S. K.; Bodner, G. *S.;* Patton, A. T.; Gladysz, J. A. *Organometallics* **1990**, *9,* 1184−1191. (e) Peng, T. S.; Gladysz, J. A. *J. Am. Chem. Soc.* **1992**, *114*, 4174−4181. (f) Schmidt, G. F.; Brookhart, M. *J. Am. Chem. Soc.* **1985**, *107,* 1443−1444.

MA050959C